Efficient Visible-to-Ultraviolet Photon Upconversion using Excited Triplet States in Molecular Diffusion Systems

原田, 直幸

Efficient Visible-to-Ultraviolet Photon Upconversion using Excited Triplet States in Molecular Diffusion Systems

Naoyuki Harada

Department of Applied Chemistry

Graduate School of Engineering

Kyushu University

2023

Efficient Visible-to-Ultraviolet Photon Upconversion using Excited Triplet States in Molecular Diffusion Systems

Author

Naoyuki Harada

Supervisor

Nobuo Kimizuka

Department of Applied Chemistry

Graduate School of Engineering, Kyushu University

December 2023

KYUSHU
UNIVERSITY

Acknowledgments

The study in this thesis was carried out under the supervision of Professor Nobuo Kimizuka from April 2018 at the Department of Applied Chemistry, Graduate School of Engineering, Kyushu University.

I would like to express my deepest gratitude to Professor Nobuo Kimizuka for giving me an invaluable opportunity and experience in his laboratory and guiding me with precious suggestions. I would also like to thank Associate Professor Nobuhiro Yanai for his helpful advice and the opportunity to learn how to research. I am deeply grateful to Assistant Professor Masa-aki Morikawa, Assistant Professor Yoichi Sasaki, Professor Shigenori Fujikawa, Professor Teppei Yamada (The University of Tokyo), Assistant Professor Joseph Ka Ho Hui, and Assistant Professor Kiichi Mizukami for their advice and suggestions during my research. I am also grateful to Professor Tsuyohiko Fujigaya and Professor Takuma Yasuda for reviewing my dissertation.

I am greatly indebted to the Japan Society for the Promotion of Science (JSPS) for financial support (Research Fellowship for Young Scientists and JSPS KAKENHI).

I want to thank Ms. Kazumi Matsuno, Ms. Ryo Maeda, Ms. Chihoko Fukakusa, Dr. Shota Hisamitsu, Dr. Masanori Hosoyamada, Dr. Tsubasa Kashino, Dr. Yimin Liang, Dr. Hironori Kouno, Dr. Keisuke Okumura, Dr. Ryosuke Yamamoto, Dr. Saiya Fujiwara, Dr. Yuki Nagai, Dr. Yusuke Kawashima, Mr. Zheng Yan, Mr. Junji Miyano, Ms. Nao Hirakawa, Ms. Rena Haruki, Ms. Mika Kinoshita, Mr. Takashi Kobayashi, Mr. Tetsuro Kobayashi, Mr. Keisuke Hayashi, and Dr. Koki Nishimura for their warm supports and discussion. I want to offer my thanks to Mr. Masanori Uji, Mr. Mai Lam Bac, Mr. Yuya Watanabe, and Mr. Hayato Shoyama for helpful discussion and for giving me an opportunity to improve myself. I am also grateful to all members who worked together in Kimizuka Lab: Dr. Pankaj Bharmoria, Dr. Biplab Joarder, Dr. Tejwant Singh, Dr. Arijit Mallick, Dr. Gurbir Singh, Dr. Baljeet Singh, Dr. Ilias Papadopoulos, Dr. Keita Kuge, Mr. Hirotaka Inoue, Ms. Risa Iwami, Ms. Kana Orihashi, Mr. Donggyu Kwak, Ms. Mio Koharagi, Ms. Mone Sakata, Mr. Yuichiro Seki, Mr. Issei Maruyama, Ms. Kanae Izumi, Mr. Jumpei Kondo, Mr. Kentaro Tanaka, Mr. Ryoichi Tomomatsu, Mr. Tomoyuki Hamachi, Mr. Fumitoshi Matoba, Mr. Akio Yamauchi, Mr. Shuta Waki, Ms. Naura Fakhira Antariksa, Ms. Hikari Ishihara, Ms. Tae Tamemoto, Mr. Udai Danyoshi, Mr. Yuma Nakashima, Ms. Yuka Masunaga, Mr. Naoto Matsumoto, Mr. Keita Sakamoto, Mr. Kodai Matsumoto, Mr. Reiya Yabuki, Mr. Yuta Yamanaka, Mr. Masis Sirim, Mr. Zhu Junzhe, Mr. Issa Takatsuka, Ms. Miko Mizuno, Ms. Miku Inoue, Mr. Yusei Sawada, Mr. Yuta Sawada, Ms. Boonmong Nutnicha, Ms. Aki Masaoka, and Mr. Sauer Adrian.

Finally, I thank my family for their warm encouragement and continuous support.

Naoyuki Harada

Department of Applied Chemistry

Graduate School of Engineering, Kyushu University

December 2023

Table of Contents

Chapter 1 Introduction

1-1 Solar energy and ultraviolet (UV) light

Sunlight is a natural energy source we can sustainably use to live on Earth. Sunlight contains light ranging from ultraviolet (UV) to infrared (IR), with different intensity distributions (Figure 1-1).[1] For example, ~3% is UV light, which has high energy for sunburn and disinfection, ~45% is visible light, and ~52% is IR light, which has skin-penetrating and heat-generating effects.[1, 2]

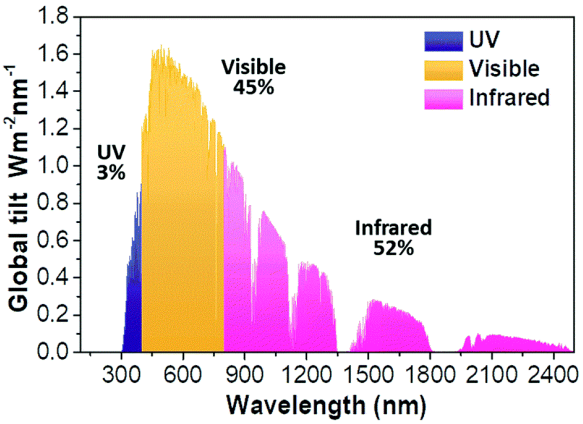

Figure 1-1 Solar irradiance (AM1.5). Adapted with permission from Ref. [1]. Copyright 2019 the Royal Society of Chemistry.

In particular, high-energy (short-wavelength) UV light is vital as a driving force for photocatalysts such as titanium dioxide (TiO_2) and photocatalytic reactions (Figure 1-2a).[3, 4] However, sunlight does not contain much UV light. Therefore, materials that can absorb visible light have been developed in the field of photocatalysts.[5-7] On the other hand, a method called photon upconversion (UC), which can convert visible light, abundant in sunlight, into UV light, has also been studied (Figure 1-2b, c).[8]

1-2 Photon upconversion (UC)

Photon upconversion is a methodology for converting low-energy (long-wavelength) light into high-energy (short-wavelength) light. Typical mechanisms include two-photon absorption (TPA), multi-step excitation in lanthanide-containing materials, and triplet-triplet annihilation (TTA).

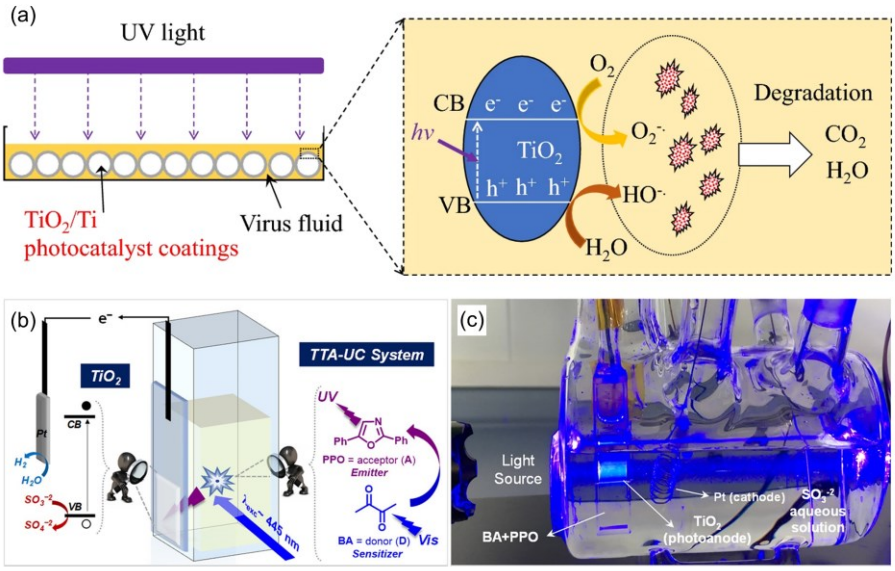

Figure 1-2 (a) Proposed mechanisms of viral inactivation induced by TiO_2/Ti photocatalyst coatings. Adapted with permission from Ref. [4]. Copyright 2022 Springer Nature. (b) Selective visible light irradiation to the TTA-UC system releases UV emission that activates TiO_2, generating a photocurrent. (c) Photograph of the TTA-UC-powered PEC cell. Adapted with permission from Ref. [8]. Copyright 2018 American Chemical Society.

1-2-1 Two-photon absorption (TPA)

Two-photon absorption (TPA) is a phenomenon in which a molecule continuously absorbs two photons, generating a state with energy higher than the excitation wavelength (Figure 1-3).[9, 10] Because of its high spatial resolution, TPA has been applied as a microscopy technique. It is possible to image deep into biological tissues non-invasively using near-infrared light, which has high biological transparency. However, it is generally difficult to effectively use sunlight because it requires high-power laser light with an excitation intensity of W cm^{-2} or higher.

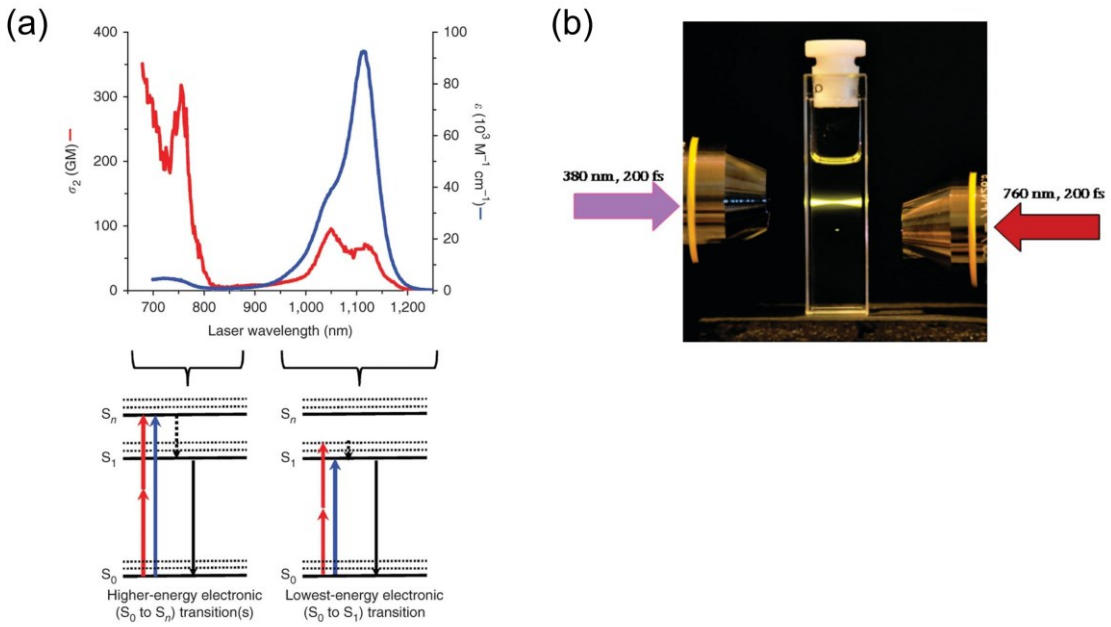

Figure 1-3 (a) One-photon absorption and two-photon absorption spectra of TagRFP as anionic chromophore, and energy diagram of one-photon absorption and TPA transitions. Adapted with permission from Ref. [10]. Copyright 2011 Springer Nature. (b) Photograph of one-photon (purple arrow) versus two-photon (red arrow) excitation, showing the high 3D spatially localized excitation. Adapted with permission from Ref. [9]. Copyright 2010 American Chemical Society.

1-2-2 Multi-step excitation in lanthanide-containing materials

Lanthanide-containing nanoparticles (UCNPs) such as erbium (Er), thulium (Tm), and ytterbium (Yb) can harvest near-infrared light at wavelengths around 980 nm and exhibit upconversion through a multi-step mechanism (Figure 1-4),[11, 12] and have potential applications in bioimaging and photovoltaics, despite the typically low quantum yield (< 10%) of UC, which is still far from sunlight-based applications.

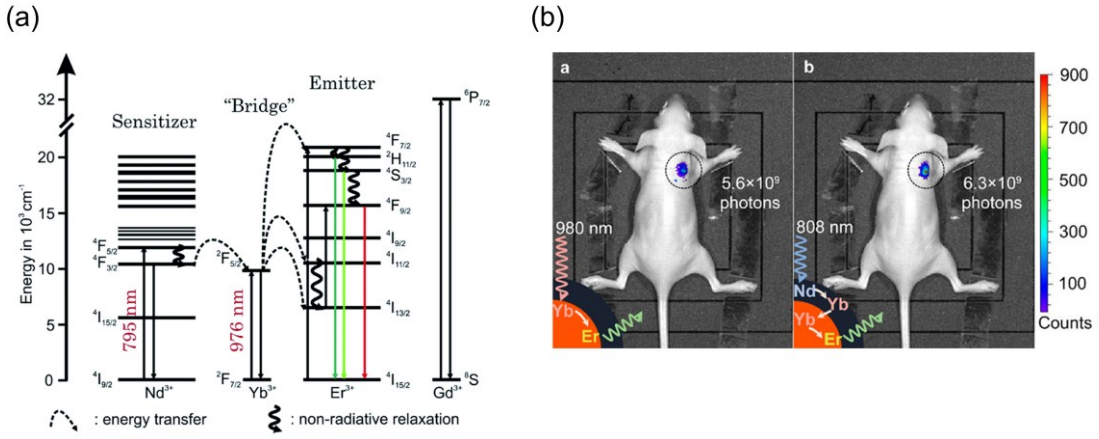

Figure 1-4 (a) Schematic energy diagram of the upconversion mechanism of a Yb^{3+} and Er^{3+} dopant ion system (λ_{ex} = 976 nm) and the mechanism of a Nd^{3+}, Yb^{3+} and Er^{3+} dopant ion system (λ_{ex} = 795 nm). Adapted with permission from Ref. [12]. Copyright 2015 the Royal Society of Chemistry. (b) In vivo UC imaging of a nude mouse subcutaneously injected with Er@Nd NPs (980 and 808 nm laser excitation). Adapted with permission from Ref. [11]. Copyright 2013 American Chemical Society.

1-2-3 Triplet-triplet annihilation (TTA)

Triplet-triplet annihilation (TTA) is a phenomenon that occurs when the triplet states of two organic molecules interact. Although the triplet state is weak against oxygen molecules and has a modest wavelength conversion shift, it can utilize weak light at the solar level (mW cm^{-2}) and has high UC quantum yields, making it promising for applications in solar cells and biological imaging (Figure 1-5).[13, 14]

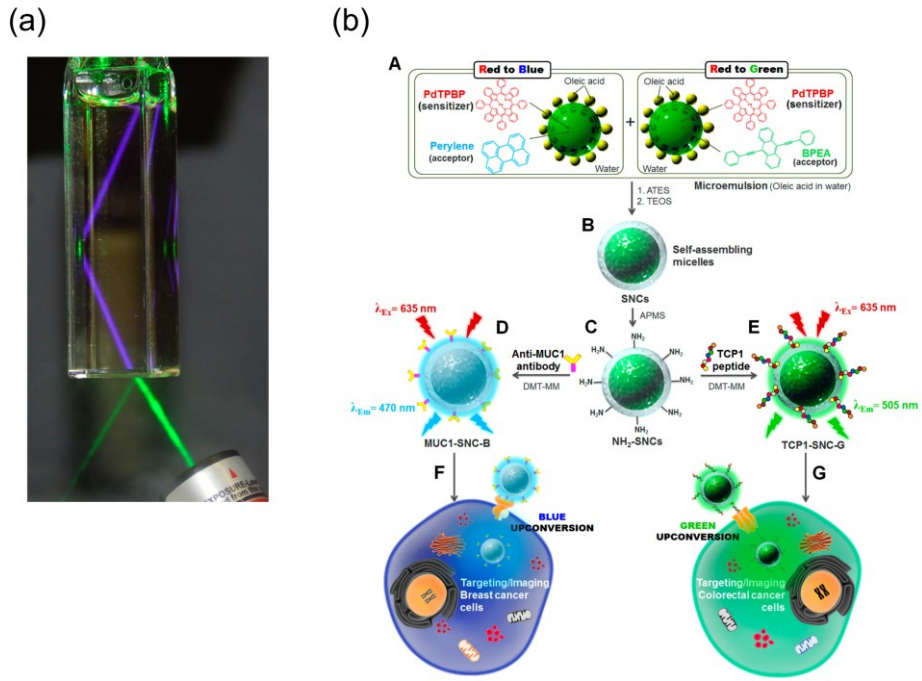

Figure 1-5 (a) Photograph of upconverted emission in a CH_3CN solution containing $[Ru(dmb)_3]^{2+}$ and 9,10-diphenylanthracene under a commercial green laser pointer (λ_{ex} = 532 nm). Adapted with permission from Ref. [13]. Copyright 2010 Elsevier. (b) A procedure to fabricate bioprobe-attached silica nanocapsules (SNC) and the schematic illustration of cancer bioimaging. Adapted with permission from Ref. [14]. Copyright 2016 American Chemical Society.

1-3 TTA-based photon upconversion (TTA-UC)

TTA was first reported in the 1960s by C. A. Parker and C. G. Hatchard.[15-18] In the 2000s, TTA-UC, led by F. N. Castellano, was brought to the attention again.[13]

1-3-1 General mechanism of TTA-UC

TTA-UC occurs through a multi-step reaction combining two types of molecules, a donor (triplet sensitizer) and an acceptor (emitter), as shown in the figure below (Figure 1-6).

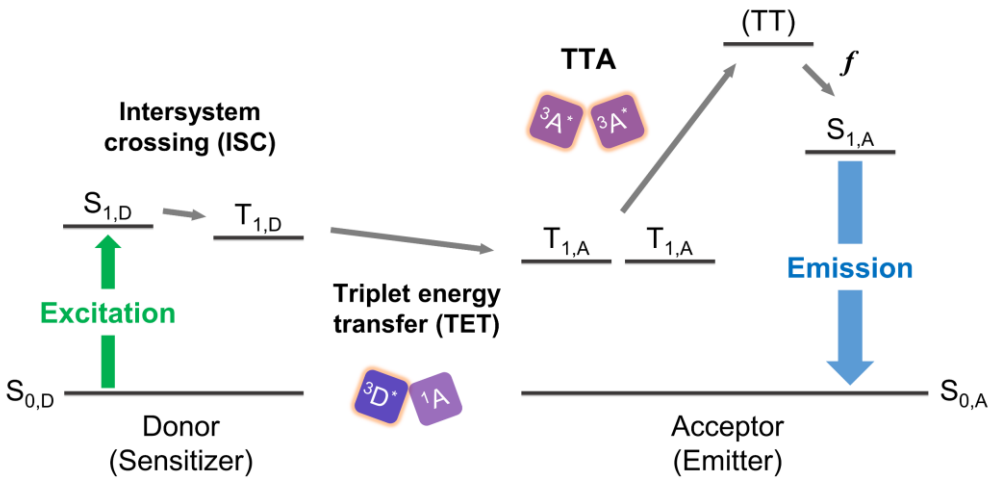

Figure 1-6 The mechanism of TTA-UC. S and T indicate singlet and triplet states, respectively. Upconverted emission is obtained through a triplet pair (TT) with a singlet generation efficiency (f).

First, the donor absorbs light, generating the excited singlet state of the donor ($S_{1,D}$). The excited triplet state of the donor ($T_{1,D}$) is then formed by intersystem crossing (ISC). The triplet energy of the donor is transferred to the acceptor, which is called triplet energy transfer (TET), generating the triplet state of the acceptor ($T_{1,A}$). The induced triplet state of the acceptor diffuses through the medium, such as organic solvents and polymers during its triplet lifetime, and molecular collisions between acceptors cause triplet-triplet annihilation, thus forming the excited singlet state of the acceptor ($S_{1,A}$). In the mechanism, since TET and TTA occur by an electron exchange mechanism known as the Dexter mechanism, the distance between the molecules must be within about 1 nm. Furthermore, as discussed later (see 1-3-2-1), the TTA process involves a triplet pair (TT) as an intermediate, which contributes significantly to TTA-UC efficiency.

1-3-2 Basic parameters of TTA-UC

1-3-2-1 TTA-UC efficiency

The efficiency of TTA-UC (η_{UC}) is expressed by the following equation,[19]

$$\eta_{UC} = f\Phi_{ISC}\Phi_{TET}\Phi_{TTA}\Phi_{FL} \quad \text{(Eq. 1-1)}$$

where f is the spin statistical factor (singlet generation efficiency), Φ_{ISC}, Φ_{TET}, Φ_{TTA}, and Φ_{FL} are the efficiencies of ISC, TET, TTA, and acceptor fluorescence, respectively. It is noticed that, in principle, a TTA-UC quantum yield (Φ_{UC}) with a maximum value of 50% can be obtained, but here, the efficiency of TTA-UC (η_{UC}) normalized to 100% is used.[20] As seen from the equation (Eq. 1-1), the efficiency of TTA-UC is expressed as the product of the efficiency of each process. Since Φ_{ISC}, Φ_{TET}, Φ_{TTA}, and Φ_{FL} can be made unity by combining the appropriate chromophores, the actual TTA-UC is controlled by the f value.

The spin statistic rule governs the f value, and 40% (2/5) is typically considered the maximum value (Figure 1-7a).[21] This is based on the idea that the singlet and triplet states are formed in a 1:3 ratio from the triplet pair, with the triplet state again involved in the TTA. Recently, it was reported that under certain conditions of molecular orientation, the f value can achieve up to 66% (Figure 1-7b).[22] It is also predicted that the f value as high as 100% can be achieved if the generated highly-lying excited triplet state can be converted to the singlet state. Although many f values have been reported using a variety of dyes, most have remained below 40% except for a few systems (Figure 1-8).[23, 24]

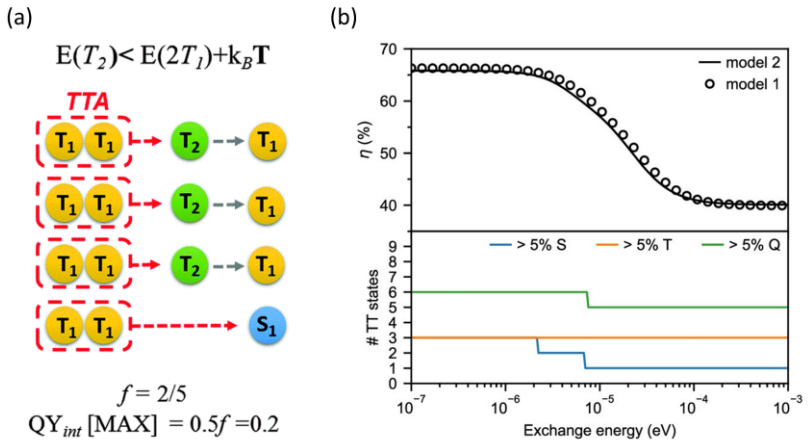

Figure 1-7 (a) Illustration of how to obtain a conventional f value of 40%, in which T_2 levels are energetically recyclable. Adapted with permission from Ref. [21]. Copyright 2015 the Royal Society of Chemistry. (b) Simulated spin statistical factor as η for parallel molecules as a function of inter triplet exchange energy, indicating that the f value is achievable up to 66%. Adapted with permission from Ref. [22]. Copyright 2021 American Chemical Society.

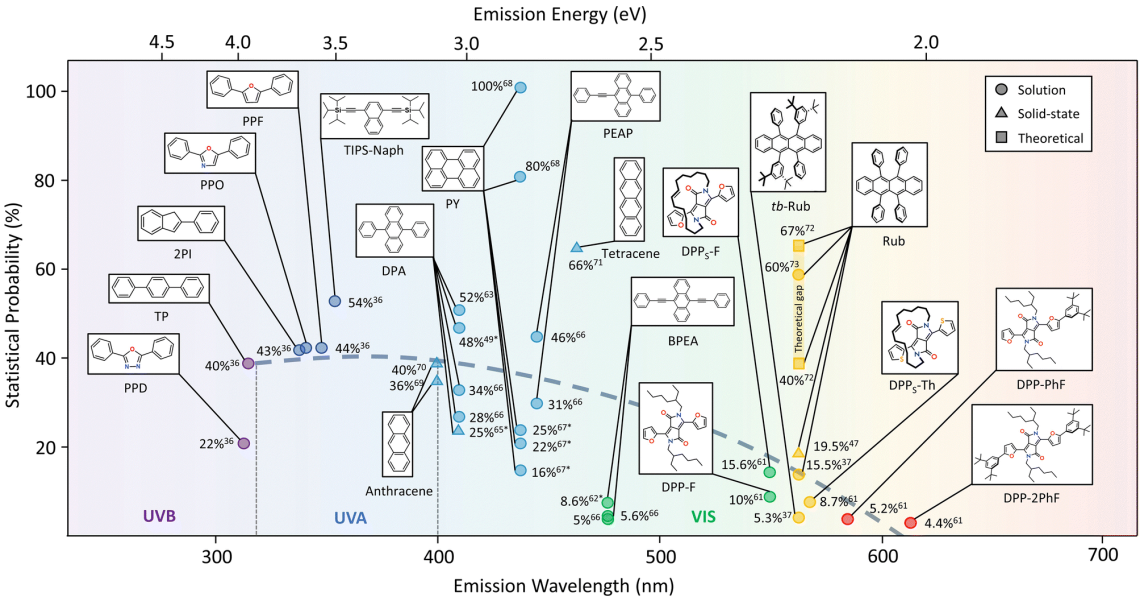

Figure 1-8 Spin statistical factor values in solution (circle), solid-state (triangle), and the values calculated theoretically (square). Reproduced with permission from Ref. [23]. Copyright 2023 the Royal Society of Chemistry and the Chinese Chemical Society.

1-3-2-2 Threshold excitation intensity

The following equation describes the dynamics of TTA-UC.[25]

$$\frac{\partial T_{\mathrm{D}}}{\partial t} = \alpha(\mathrm{E})I_{\mathrm{exc}} - k_{\mathrm{D}}^{\mathrm{T}}T_{\mathrm{D}} - k_{\mathrm{tr}}T_{\mathrm{D}} \qquad \text{(Eq. 1-2)}$$

$$\frac{\partial T_{\mathrm{A}}}{\partial t} = k_{\mathrm{tr}}T_{\mathrm{D}} - k_{\mathrm{A}}^{\mathrm{T}}T_{\mathrm{A}} - \gamma_{\mathrm{TT}}{T_{\mathrm{A}}}^{2} \qquad \text{(Eq. 1-3)}$$

$$\frac{\partial S_{\mathrm{A}}}{\partial t} = 0.5f\gamma_{\mathrm{TT}}{T_{\mathrm{A}}}^{2} - k_{\mathrm{A}}^{\mathrm{S}}S_{\mathrm{A}} \qquad \text{(Eq. 1-4)}$$

where T_{D}, T_{A}, and S_{A} are the population of the donor triplets, the acceptor triplets, and the acceptor singlets, respectively. The parameter $\alpha(\mathrm{E})$ is the donor absorption coefficient, and I_{exc} is the excitation power density. The rate constants $k_{\mathrm{D}}{}^{\mathrm{T}}$, $k_{\mathrm{A}}{}^{\mathrm{T}}$, $k_{\mathrm{A}}{}^{\mathrm{S}}$, k_{tr}, and γ_{TT} indicate a spontaneous decay of the donor triplet, a nonradiative decay of the acceptor triplet, a decay of the acceptor singlet, the energy transfer from the donor to the acceptor, and the second-order decay characterizing the TTA process. The f is the spin statistical factor for generating the acceptor singlet from the TTA process. Under the steady-state conditions at low excitation power where the TTA process is negligible ($k_{\mathrm{A}}{}^{\mathrm{T}}T_{\mathrm{A}} \gg \gamma_{\mathrm{TT}}T_{\mathrm{A}}{}^{2}$), the S_{A} is expressed by the following equation,

$$S_{\mathrm{A}} = 0.2\frac{\gamma_{\mathrm{TT}}}{k_{\mathrm{A}}^{\mathrm{S}}}\left[\frac{k_{\mathrm{tr}}/k_{\mathrm{A}}^{\mathrm{T}}}{k_{\mathrm{D}}^{\mathrm{T}} + k_{\mathrm{tr}}}\right]^{2}[\alpha(\mathrm{E})I_{\mathrm{exc}}]^{2} \propto {I_{\mathrm{exc}}}^{2} \qquad \text{(Eq. 1-5)}$$

which indicates that the upconverted PL intensity is quadratic to the excitation power density since it is proportional to the S_{A}. On the other hand, at high excitation power density where the triplet-triplet annihilation is the dominant channel ($\gamma_{\mathrm{TT}}T_{\mathrm{A}}{}^{2} \gg k_{\mathrm{A}}{}^{\mathrm{T}}T_{\mathrm{A}}$), the S_{A} is obtained as a function of the excitation power density below.

$$S_{\mathrm{A}} = 0.2\frac{1}{k_{\mathrm{A}}^{\mathrm{S}}}\left[\frac{k_{\mathrm{tr}}}{k_{\mathrm{D}}^{\mathrm{T}} + k_{\mathrm{tr}}}\right]\alpha(\mathrm{E})I_{\mathrm{exc}} \propto I_{\mathrm{exc}} \qquad \text{(Eq. 1-6)}$$

In this condition, S_{A} and upconverted PL intensity are proportional to the excitation power density. These trends of the upconverted PL intensity are shown in a double-logarithm plot versus excitation power density (Figure 1-9).[26]

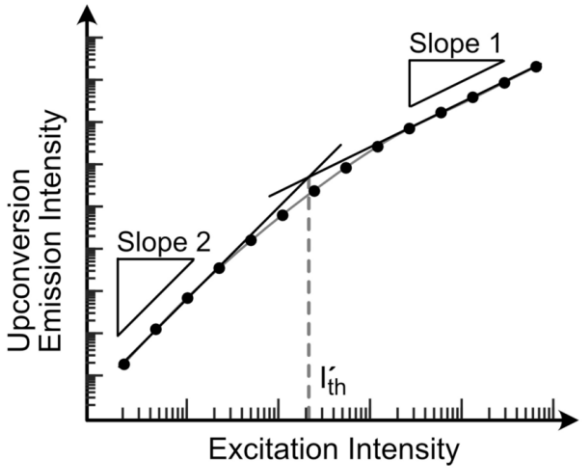

Figure 1-9 The excitation intensity dependence of upconverted emission intensity in a double-logarithm plot. Adapted with permission from Ref. [26]. Copyright 2022 Springer Nature.

From Eq. 1-5 and 1-6, the power density at which the S_A becomes equal concentrations ($k_A{}^T T_A = \gamma_{TT} T_A{}^2$), the threshold excitation intensity (I_{th}) is defined by the following equation,

$$I_{\mathrm{th}} = \frac{1}{\Phi_{\mathrm{TET}} \alpha(\mathrm{E}) \gamma_{\mathrm{TT}} {\tau_{\mathrm{T}}}^2} \qquad \text{(Eq. 1-7)}$$

where Φ_{TET} is defined as a quantum yield of the triplet energy transfer by $\Phi_{\mathrm{TET}} = k_{\mathrm{tr}} / \left(k_{\mathrm{tr}} + k_{\mathrm{D}}^{\mathrm{T}}\right)$ and τ_T is the lifetime of the acceptor triplet by $\tau_{\mathrm{T}} = 1/k_{\mathrm{A}}^{\mathrm{T}}$. This relationship shows that the I_{th} is inversely proportional to Φ_{TET}, α(E), γ_{TT}, and the square of τ_T. In the double-logarithm plot, the I_{th} is experimentally obtained as the intersection of two linear lines with slopes 2 and 1, and the I_{th} is used as an indicator to optimize the upconversion system in terms of excitation intensity.[25, 27, 28] Recently, as another method to calculate the I_{th}, the theoretical fitting model has been reported, enabling us to estimate the I_{th} more efficiently with less subjectivity.[29] They also reported that the I_{th} calculated by the intersection shows an excitation intensity in which 38.2% of the maximum η_{UC} is obtained, not 50%. The equation (Eq. 1-7) provides how to optimize the TTA-UC system. The triplet lifetime of the acceptor has a significant impact on I_{th}. Thus, an excellent acceptor should have a long triplet lifetime. In a three-dimensional diffusion system, γ_{TT} can be expressed by the following equation,

$$\gamma_{TT} = 8\pi a_0 D_{\mathrm{T}} \qquad \text{(Eq. 1-8)}$$

in which a_0, and D_T are an effective intermolecular distance for TTA and a diffusion constant of the acceptor triplet, respectively. From the above equation, the diffusion constant must also be considered to control the I_{th} (Figure 1-10).[30] The triplet diffusion constant in a solution system can be equal to the diffusion constant of the acceptor molecule.

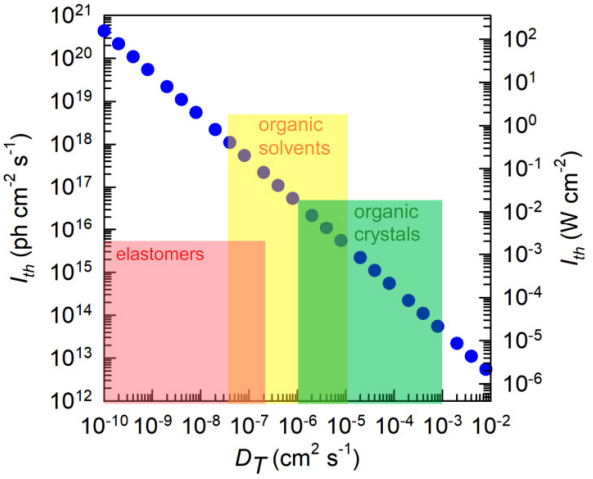

Figure 1-10 Threshold excitation intensity calculated as a function of the diffusion constant of an acceptor triplet considering α = 10 cm^{-1}, Φ_{TET} = 100%, a triplet decay rate of 1 kHz, and excitation wavelength at 532 nm. Adapted with permission from Ref. [30]. Copyright 2021 AIP Publishing.

1-4 The current trend of visible-to-UV TTA-UC

While photon upconversion systems based on TTA for the conversion of visible light into UV light are beneficial for some applications described above (see 1-1), the efficiency of visible-to-UV TTA-UC systems has been limited, and the number of reports is smaller than that of the reported systems for visible-to-visible and near-IR-to-visible TTA-UC.

1-4-1 Solution systems

Visible-to-UV TTA-UC systems in solution have been researched since the early 2000s (Table 1-1).[31-34] In 2006, W. Zhao and F. N. Castellano reported a system using di-*tert*-butylpyrene (DBP) and Ir(ppy)$_3$ that shows pyrene emission under a 450 nm excitation.[34] Pyrene, 2,5-diphenyloxazole (PPO), *p*-quarterphenyl (QP), and *p*-terphenyl (TP) are well-known UV-emitting acceptors (Figure 1-11).[8, 34-49] However, the systems using these acceptors suffered from low TTA-UC efficiencies below 10%, except for two reported values. In 2017, a 5.2% efficiency was reported using PPO as the acceptor and CdS/ZnS core-shell nanocrystals (NCs) as the donor by V. Gray *et al*.[43] S. He *et al*. reported a 10.2% efficiency using PPO as the acceptor and CsPbBr$_3$ perovskite NCs as the donor in 2019.[45]

Table 1-1 Reported systems for visible-to-UV TTA-UC in solution. The η_{UC} and I_{th} written are representative values for each system.

Year[Ref.]	Donor	Acceptor	η_{UC} (%)	I_{th} (mW cm^{-2})	Solvent
2006[34]	$Ir(ppy)_3$	Pyrene	-	-	CH_2Cl_2
2006[34]	$Ir(ppy)_3$	3,8-DBP	-	-	CH_2Cl_2
2009[41]	Biacetyl	PPO	1.16	-	Benzene
2014[35]	$Ir(C6)_2(acac)$	2,7-DBP	2.0	0.78	DMF
2015[36]	$Ir(C6)_2(acac)$	2,7-DBP	-	28	DMF gel
2015[42]	Biacetyl	PPO	0.24	-	DMF
2016[47]	4CzIPN	QP	3.9	775	Benzene
2016[47]	4CzIPN	TP	2.8	$> 1 \times 10^3$	Benzene
2016[37]	4CzPN	2,7-DBP	4.4	-	Toluene
2016[37]	4CzPN-1DBP	2,7-DBP	3.7	-	Toluene
2017[43]	CdS/ZnS/NCA	PPO	5.2	-	Hexane
2017[38]	$[Ru(bpy)_3]^{2+}$	$PyCO_2^-$	-	$> 2 \times 10^3$	Water
2018[39]	4CzPN-DBP	2,7-DBP	1.7	-	Toluene
2018[8]	Biacetyl	PPO	-	-	DMF
2019[44]	$CsPbX_3$/NCA	PPO	> 4	4.7×10^3	Toluene
2019[40]	4CzIPN	Pyrene	0.66	$> 2 \times 10^3$	Oleic acid/THF
2019[45]	$CsPbBr_3$/NCA	PPO	10.2	$\sim 1.9 \times 10^3$	Hexane
2019[46]	$Ir(ppy)_3$	P_{66614}PPOS	0.44	61	Ionic liquid
2020[48]	FIrpic/Dec	Amphiphile TP	0.1	$> 4 \times 10^3$	Water
2020[50]	IrFsppy	NDS	~0.07	-	Water
2020[51]	$Ir(C6)_2(acac)$	TIPS-Nph	20.5	1.1	THF

NCA: 1-Naphthoic acid

$PyCO_2^-$: 1-Pyrenecarboxylate

P_{66614}: Trihexyltetradecylphosphonium

PPOS: 4-(2-Phenyloxazol-5-yl)benzenesulfonate

NDS: 1,5-Naphthalenedisulfonate

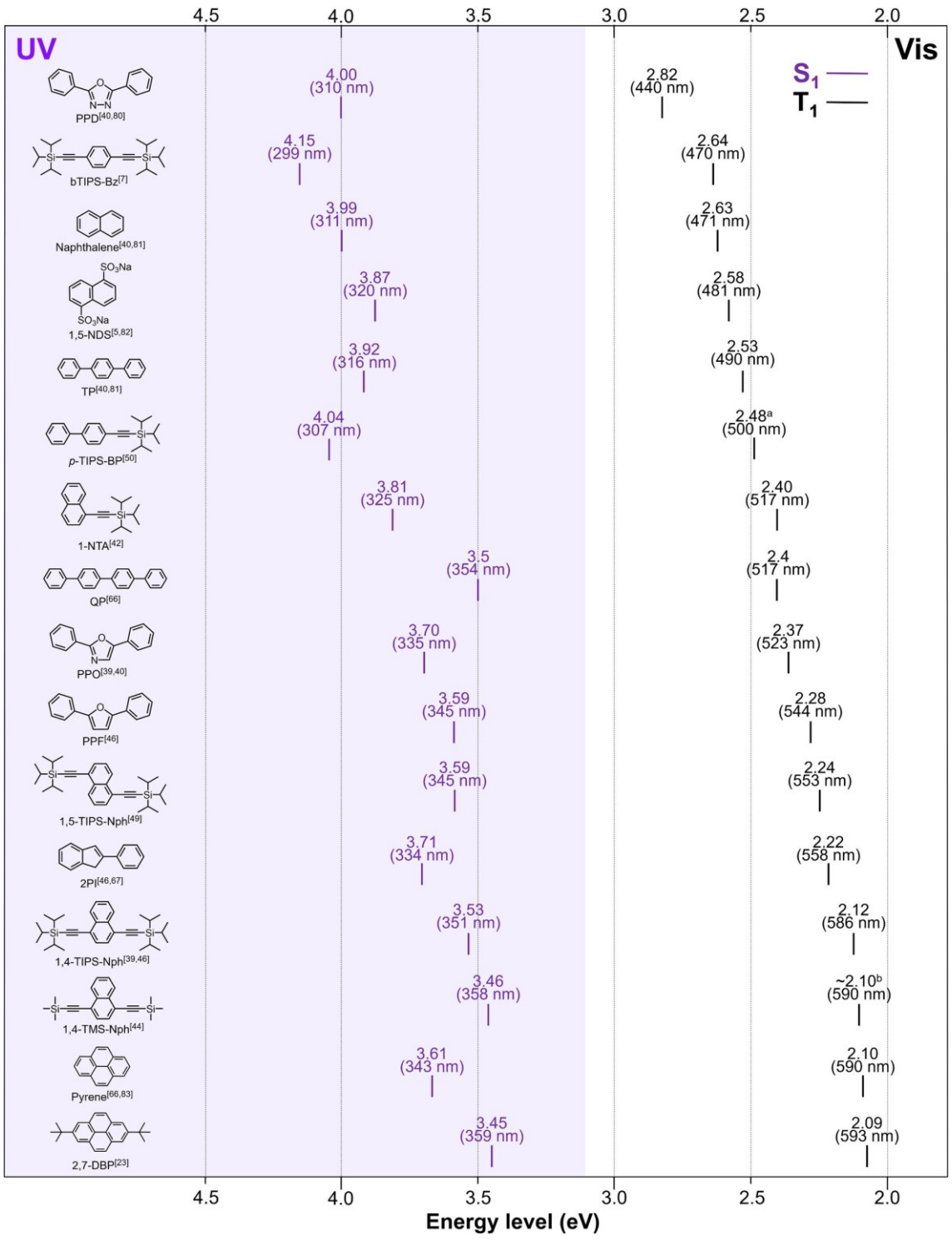

Figure 1-11 Energy levels of excited singlet and triplet states of acceptors, including estimated by DFT calculations and anticipated values. Reproduced with permission from Ref. [52]. Copyright 2023 John Wiley and Sons.

The threshold excitation intensity (I_{th}) and the efficiency were not efficient enough to be applied for solar applications. Most systems showed a high I_{th} value above 10^2 mW cm^{-2}, one magnitude higher than sunlight. The system using DBP as the acceptor and Ir(C6)$_2$(acac) as the donor showed an exceptionally low value of 0.78 mW cm^{-2}, but the efficiency of TTA-UC was only up to 2.0%.[35]

In 2020, we reported TIPS-Nph,[51] which revolutionized the research field of visible-to-UV TTA-UC. The details of this TIPS-Nph are discussed in detail in Chapter 2. Since we reported TIPS-Nph, the number of reports on TTA-UC from visible to UV light has increased dramatically. Some use heavy metal-free donors or convert green light to UV light with TIPS-Nph.[53-58] The combination of TIPS-Nph and 4CzBN shows the highest η_{UC} of 26.2% at this moment.[54] Many studies have followed our work, and TIPS-Nph is becoming the standard dye in the visible-to-UV TTA-UC field (Figure 1-12, Table 1-2).

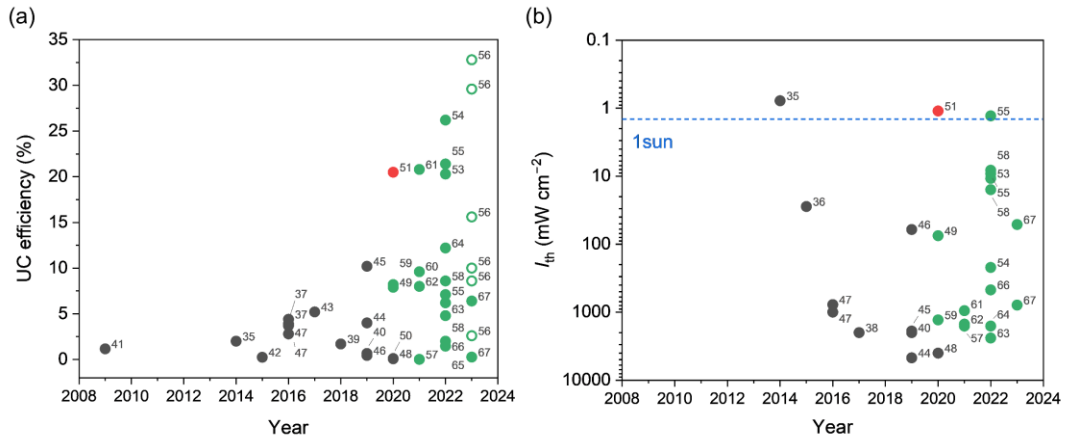

Figure 1-12 (a) TTA-UC efficiency and (b) threshold excitation intensity (I_{th}) of reported systems (1sun: 1.4 mW cm^{-2} at 445 nm ± 5 nm). The data are referred from Table 1-1 and Table 1-2. Red circles show the data from this work. The data with an open circle indicates the corrected efficiency.

Table 1-2 Reported new systems for visible-to-UV TTA-UC in solution. The η_{UC} and I_{th} written are representative values for each system.

Year[Ref.]	Donor	Acceptor	η_{UC} (%)	I_{th} (mW cm^{-2})	Solvent
2020[49]	4CzIPN	(*R*, *S*)-TP	7.9	75	Toluene
2020[59]	BCAc	DTBN	8.2	1.3×10^3	Hexane
2021[60]	$Ir(ppy)_3$	2,7-DBP	9.6	-	DMF
2021[61]	CdS/3PCA	PPO	20.8	9.5×10^2	Toluene
2021[62]	4CzIPN	*p*-TIPS-BP	8.0	~1.5×10^3	Cyclohexane/ toluene
2021[57]	$CsPbBr_3/P_{66614}$ PPOS	TIPS-Nph	0.014	1.6×10^3	Toluene
2022[53]	CBDAC	TIPS-Nph	20.3	10.8	Toluene
2022[58]	BN-2Cz	TIPS-Nph	8.6	15.8	Toluene
2022[58]	BN-2Cz-*t*Bu	TIPS-Nph	4.8	9.2	Toluene
2022[63]	ZnSe/ZnS/BCA	DTBN	6.2	2.4×10^3	Hexane
2022[64]	$CsPbBr_3$/PTA	PPO	12.2	~1.6×10^3	Hexane
2022[54]	4CzBN	TIPS-Nph	26.2	220	Toluene
2022[65]	[Zn(*m*-L)$_2$]	TMS-Nph	1.46	-	Toluene
2022[66]	4CzIPN	bTIPS-Bz	~2	471	Cyclohexane/ toluene
2022[55]	BN-Se	TIPS-Nph	21.4	1.3	Toluene
2022[55]	BN-Se	1-TNA	7.1	8.2	Toluene
2023[67]	$Ir(ppy)_2(acac)$	2,7-DBP	0.26	787	Micelle
2023[67]	$Ir(ppy)_2(acac)$, Ir(tmd)	2,7-DBP	6.4 (tmd/DBP)	51.5 (ppy_2/DBP)	Toluene
2023[68]	Biacetyl	PPO	-	-	Monomer
2023[56]	4CzBN	N-1TMS	2.6*	-	Toluene
2023[56]	4CzBN	N-1TIPS	8.6*	-	Toluene
2023[56]	4CzBN	N-1TPhS	10.0*	-	Toluene
2023[56]	4CzBN	TMS-Nph	15.6*	-	Toluene
2023[56]	4CzBN	TIPS-Nph	32.8*	-	Toluene

2023[56]	4CzBN	N-2TPhS	29.6*	-	Toluene
2023[69]	$[Ru(bpy)_3]^{2+}$	Pyrene	-	-	Aqueous SDS solution

*Calculated value using generated UC quantum yields ($\Phi_{UC,g}$)

BCAc: 10-Butyl-2-chloro-9(10*H*)-acridinone

DTBN: 2,6-Di-*tert*-butylnaphthalene

PCA: Phenanthrene-3-carboxylic acid

CBDAC: 3,3'-Carbonylbis(7-diethylaminocoumarin)

BCA: 4-Biphenylcarboxylic acid

PTA: 9-Phenanthrenecarboxylic acid

1-TNA: Triisopropyl(naphthalen-1-ylethynyl)silane

TMS-Nph: 1,4-Bis((trimethylsilyl)ethynyl)naphthalene

1-4-2 Film and solid systems

In contrast to TTA-UC in solution, few studies of film and solid systems have been reported (Table 1-3).[39, 70-72] The first report of blue-to-UV TTA-UC was performed in rigid poly(methyl methacrylate) (PMMA) films containing PPO and 2-methoxythioxanthone (2MeOTX) by P. B. Merkel and J. P. Dinnocenzo in 2008.[70] Y. Ma and co-workers then reported Polyurethane (PU) systems containing DBP.[39, 71] In 2022, R. Enomoto and Y. Murakami reported the neat film of PPO containing CBDAC as the donor, and this system showed the highest η_{UC} of up to 8.6% with relatively low I_{th} values at 13.8−17.0 mW cm^{-2}.[72] For practical application of visible-to-UV TTA-UC, it is necessary to develop film- and solid-state systems in the future.

Table 1-3 Reported systems for visible-to-UV TTA-UC in film and solid. The η_{UC} and I_{th} written are representative values for each system.

Year[Ref.]	Donor	Acceptor	η_{UC} (%)	I_{th} (mW cm^{-2})	Matrix
2008[70]	2MeOTX	PPO	-	-	PMMA
2016[71]	Ir(ppy-DBP)	2,7-DBP	2.6	-	Polyurethane
2016[37]	4CzPN-1DBP	2,7-DBP	-	-	Polyurethane
2022[72]	CBDAC	PPO	8.6	13.8	Neat PPO

1-5 Overview of the thesis

The main objective of this thesis is to establish efficient TTA-UC systems based on molecular diffusion to convert visible light into UV light. This chapter describes the essential characteristics of TTA-UC and the current situation of visible-to-UV TTA-UC.

Chapter 2 describes the details of efficient visible-to-UV TTA-UC using TIPS-Nph and $Ir(C6)_2(acac)$ in solution.[51] This system shows a high efficiency of TTA-UC (20.5%), which is two times higher than the reported value. In addition to the efficiency, a pair of TIPS-Nph and $Ir(C6)_2(acac)$ achieves a lower threshold excitation intensity of 1.1 mW cm^{-2} than 1sun.

Chapter 3 describes a new, simple method to fabricate efficient TTA-UC films using a porous film and a low-volatile TTA-UC solution.[73] The film prepared using this porous film impregnation method shows efficient TTA-UC properties with a high TTA-UC efficiency of 27.6% and a relatively low threshold excitation intensity of 20.4 mW cm^{-2}. Furthermore, the film can be combined with a microlens array, which focuses the excitation light onto the film, achieving a low threshold value of less than 0.60 mW cm^{-2}, at least one order of magnitude lower than sunlight.

Chapter 4 summarizes the thesis and describes future remarks.

1-6 References

[1] M. Gao, L. Zhu, C. K. Peh and G. W. Ho, *Energy Environ. Sci.*, 2019, **12**, 841-864.

[2] C. Chen, Y. Kuang and L. Hu, *Joule*, 2019, **3**, 683-718.

[3] T. Takata, J. Jiang, Y. Sakata, M. Nakabayashi, N. Shibata, V. Nandal, K. Seki, T. Hisatomi and K. Domen, *Nature*, 2020, **581**, 411-414.

[4] Y. Lu, S. Guan, L. Hao, H. Yoshida, S. Nakada, T. Takisawa and T. Itoi, *Sci. Rep.*, 2022, **12**, 16038.

[5] S. Banerjee, S. C. Pillai, P. Falaras, K. E. O'Shea, J. A. Byrne and D. D. Dionysiou, *J. Phys. Chem. Lett.*, 2014, **5**, 2543-2554.

[6] K. Mao, X. Wu, X. Min, Z. Huang, Y.-g. Liu and M. Fang, *Sci. Rep.*, 2019, **9**, 16321.

[7] P. Verma, A. Singh, F. A. Rahimi, P. Sarkar, S. Nath, S. K. Pati and T. K. Maji, *Nat. Commun.*, 2021, **12**, 7313.

[8] M. Barawi, F. Fresno, R. Pérez-Ruiz and V. A. de la Peña O'Shea, *ACS Appl. Energy Mater.*, 2019, **2**, 207-211.

[9] C. D. Andrade, C. O. Yanez, L. Rodriguez and K. D. Belfield, *J. Org. Chem.*, 2010, **75**, 3975-3982.

[10] M. Drobizhev, N. S. Makarov, S. E. Tillo, T. E. Hughes and A. Rebane, *Nat. Methods.*, 2011, **8**, 393-399.

[11] Y.-F. Wang, G.-Y. Liu, L.-D. Sun, J.-W. Xiao, J.-C. Zhou and C.-H. Yan, *ACS Nano*, 2013, **7**, 7200-7206.

[12] D. T. Klier and M. U. Kumke, *RSC Adv.*, 2015, **5**, 67149-67156.

[13] T. N. Singh-Rachford and F. N. Castellano, *Coord. Chem. Rev.*, 2010, **254**, 2560-2573.

[14] O. S. Kwon, H. S. Song, J. Conde, H.-i. Kim, N. Artzi and J.-H. Kim, *ACS Nano*, 2016, **10**, 1512-1521.

[15] C. A. Parker and C. G. Hatchard, *Proc. Chem. Soc. London*, 1962, 147.

[16] C. A. Parker and C. G. Hatchard, *Proc. R. Soc. Lond. A, Math. Phys. Sci.*, 1962, **269**, 574-584.

[17] C. A. Parker and C. G. Hatchard, *Proc. Chem. Soc. London*, 1962, 386-387.

[18] C. A. Parker, *Proc. R. Soc. Lond. A, Math. Phys. Sci.*, 1963, **276**, 125-135.

[19] A. Monguzzi, R. Tubino, S. Hoseinkhani, M. Campione and F. Meinardi, *Phys Chem Chem Phys*, 2012, **14**, 4322-4332.

[20] Y. Zhou, F. N. Castellano, T. W. Schmidt and K. Hanson, *ACS Energy Lett.*, 2020, **5**, 2322-2326.

[21] S. Hoseinkhani, R. Tubino, F. Meinardi and A. Monguzzi, *Phys. Chem. Chem. Phys.*, 2015, **17**, 4020-4024.

[22] D. G. Bossanyi, Y. Sasaki, S. Wang, D. Chekulaev, N. Kimizuka, N. Yanai and J. Clark, *JACS Au*, 2021, **1**, 2188-2201.

[23] L. Naimovicius, P. Bharmoria and K. Moth-Poulsen, *Mater. Chem. Front.*, 2023, **7**, 2297-2315.

[24] L. Naimovicius, E. Radiunas, M. Dapkevicius, P. Bharmoria, K. Moth-Poulsen and K. Kazlauskas, *J. Mater. Chem. C*, 2023, **11**, 14826-14832.

[25] A. Monguzzi, J. Mezyk, F. Scotognella, R. Tubino and F. Meinardi, *Phys. Rev. B*, 2008, **78**, 195112.

[26] F. Edhborg, A. Olesund and B. Albinsson, *Photochem. Photobiol. Sci.*, 2022, **21**, 1143-1158.

[27] Y. Y. Cheng, T. Khoury, R. G. C. R. Clady, M. J. Y. Tayebjee, N. J. Ekins-Daukes, M. J. Crossley and T. W. Schmidt, *Phys. Chem. Chem. Phys.*, 2010, **12**, 66-71.

[28] A. Haefele, J. Blumhoff, R. S. Khnayzer and F. N. Castellano, *J. Phys. Chem. Lett.*, 2012, **3**, 299-303.

[29] Y. Murakami and K. Kamada, *Phys. Chem. Chem. Phys.*, 2021, **23**, 18268-18282.

[30] A. Ronchi and A. Monguzzi, *J. Appl. Phys.*, 2021, **129**, 050901.

[31] D. V. Kozlov and F. N. Castellano, *Chem. Commun.*, 2004, 2860-2861.

[32] R. R. Islangulov, D. V. Kozlov and F. N. Castellano, *Chem. Commun.*, 2005, 3776-3778.

[33] R. R. Islangulov and F. N. Castellano, *Angew. Chem. Int. Ed.*, 2006, **45**, 5957-5959.

[34] W. Zhao and F. N. Castellano, *J. Phys. Chem. A*, 2006, **110**, 11440-11445.

[35] P. Duan, N. Yanai and N. Kimizuka, *Chem. Commun.*, 2014, **50**, 13111-13113.

[36] P. Duan, N. Yanai, H. Nagatomi and N. Kimizuka, *J. Am. Chem. Soc.*, 2015, **137**, 1887-1894.

[37] J. Peng, X. Guo, X. Jiang, D. Zhao and Y. Ma, *Chem. Sci.*, 2016, **7**, 1233-1237.

[38] K. A. El Roz and F. N. Castellano, *Chem. Commun.*, 2017, **53**, 11705-11708.

[39] Q. Chen, Y. Liu, X. Guo, J. Peng, S. Garakyaraghi, C. M. Papa, F. N. Castellano, D. Zhao and Y. Ma, *J. Phys. Chem. A*, 2018, **122**, 6673-6682.

[40] H.-L. Lee, M.-S. Lee, H. Park, W.-S. Han and J.-H. Kim, *Korean J. Chem. Eng.*, 2019, **36**, 1791-1798.

[41] T. N. Singh-Rachford and F. N. Castellano, *J. Phys. Chem. A*, 2009, **113**, 5912-5917.

[42] M. Majek, U. Faltermeier, B. Dick, R. Pérez‐Ruiz and A. Jacobi Von Wangelin, *Chem. Eur. J.*, 2015, **21**, 15496-15501.

[43] V. Gray, P. Xia, Z. Huang, E. Moses, A. Fast, D. A. Fishman, V. I. Vullev, M. Abrahamsson, K. Moth-Poulsen and M. L. Tang, *Chem. Sci.*, 2017, **8**, 5488-5496.

[44] K. Okumura, N. Yanai and N. Kimizuka, *Chem. Lett.*, 2019, **48**, 1347-1350.

[45] S. He, X. Luo, X. Liu, Y. Li and K. Wu, *J. Phys. Chem. Lett.*, 2019, **10**, 5036-5040.

[46] S. Hisamitsu, J. Miyano, K. Okumura, J. K.-H. Hui, N. Yanai and N. Kimizuka, *ChemistryOpen*, 2020, **9**, 14-17.

[47] N. Yanai, M. Kozue, S. Amemori, R. Kabe, C. Adachi and N. Kimizuka, *J. Mater. Chem. C*, 2016, **4**, 6447-6451.

[48] Y. Kawashima, H. Kouno, K. Orihashi, K. Nishimura, N. Yanai and N. Kimizuka, *Mol. Syst. Des. Eng.*, 2020, **5**, 792-796.

[49] D. Han, X. Yang, J. Han, J. Zhou, T. Jiao and P. Duan, *Nat. Commun.*, 2020, **11**, 5659.

[50] B. Pfund, D. M. Steffen, M. R. Schreier, M. S. Bertrams, C. Ye, K. Börjesson, O. S. Wenger and C. Kerzig, *J. Am. Chem. Soc.*, 2020, **142**, 10468-10476.

[51] N. Harada, Y. Sasaki, M. Hosoyamada, N. Kimizuka and N. Yanai, *Angew. Chem. Int. Ed.*, 2021, **60**, 142-147.

[52] M. Uji, T. J. B. Zähringer, C. Kerzig and N. Yanai, *Angew. Chem. Int. Ed.*, 2023, **62**, e202301506.

[53] M. Uji, N. Harada, N. Kimizuka, M. Saigo, K. Miyata, K. Onda and N. Yanai, *J. Mater. Chem. C*, 2022, **10**, 4558-4562.

[54] A. Olesund, J. Johnsson, F. Edhborg, S. Ghasemi, K. Moth-Poulsen and B. Albinsson, *J. Am. Chem. Soc.*, 2022, **144**, 3706-3716.

[55] X. Cao, K. Pan, J. Miao, X. Lv, Z. Huang, F. Ni, X. Yin, Y. Wei and C. Yang, *J. Am. Chem. Soc.*, 2022, **144**, 22976-22984.

[56] A. Olesund, S. Ghasemi, K. Moth-Poulsen and B. Albinsson, *J. Am. Chem. Soc.*, 2023, **145**, 22168-22175.

[57] M. Koharagi, N. Harada, K. Okumura, J. Miyano, S. Hisamitsu, N. Kimizuka and N. Yanai, *Nanoscale*, 2021, **13**, 19890-19893.

[58] Y. X. Wei, K. Pan, X. S. Cao, Y. M. Li, X. G. Zhou and C. L. Yang, *CCS Chem.*, 2022, **4**, 3852-3863.

[59] Y. Murakami, A. Motooka, R. Enomoto, K. Niimi, A. Kaiho and N. Kiyoyanagi, *Phys Chem Chem Phys*, 2020, **22**, 27134-27143.

[60] F. Glaser, C. Kerzig and O. S. Wenger, *Chem. Sci.*, 2021, **12**, 9922-9933.

[61] L. Hou, A. Olesund, S. Thurakkal, X. Zhang and B. Albinsson, *Adv. Funct. Mater.*, 2021, **31**, 2106198.

[62] T. J. B. Zähringer, M.-S. Bertrams and C. Kerzig, *J. Mater. Chem. C*, 2022, **10**, 4568-4573.

[63] X. Lin, Z. Chen, Y. Han, C. Nie, P. Xia, S. He, J. Li and K. Wu, *ACS Energy Lett.*, 2022, **7**, 914-919.

[64] S. He, Y. Han, J. Guo and K. Wu, *J. Phys. Chem. Lett.*, 2022, **13**, 1713-1718.

[65] J. A. Kübler, B. Pfund and O. S. Wenger, *JACS Au*, 2022, **2**, 2367-2380.

[66] T. J. B. Zähringer, J. A. Moghtader, M.-S. Bertrams, B. Roy, M. Uji, N. Yanai and C. Kerzig, *Angew. Chem. Int. Ed.*, 2023, **62**, e202215340.

[67] Q. Zhou, B. M. Wirtz, T. H. Schloemer, M. C. Burroughs, M. Hu, P. Narayanan, J. Lyu, A. O. Gallegos, C. Layton, D. J. Mai and D. N. Congreve, *Adv. Mater.*, 2023, **35**, 2301563.

[68] Z. Luo, D. Wang, K. Li, D. Zhong, L. Xue, Z. Gan and C. Xie, *J. Phys. Chem. Lett.*, 2023, **14**, 709-715.

[69] R. Jeyaseelan, M. Utikal, C. G. Daniliuc and L. Næsborg, *Chem. Sci.*, 2023, **14**, 11040-11044.

[70] P. B. Merkel and J. P. Dinnocenzo, *J. Lumin.*, 2009, **129**, 303-306.

[71] X. Jiang, X. Guo, J. Peng, D. Zhao and Y. Ma, *ACS Appl. Mater. Interfaces*, 2016, **8**, 11441-11449.

[72] R. Enomoto and Y. Murakami, *J. Mater. Chem. C*, 2023, **11**, 1678-1683.

[73] N. Harada, M. Uji, B. Singh, N. Kimizuka and N. Yanai, *J. Mater. Chem. C*, 2023, **11**, 8002-8006.

Chapter 2 Development of Efficient Visible-to-UV Photon Upconversion using UV-Emitting Naphthalene-Based Acceptor

2-1 Introduction

Photon upconversion based on triplet-triplet annihilation (TTA-UC) has the potential to efficiently convert low-energy photons into higher-energy photons with weak excitation light.[1-19] TTA-UC occurs in multi-chromophore systems with a donor (sensitizer) and an acceptor (emitter), in which the triplet energy is transferred from the donor to the acceptor, followed by annihilation among the acceptors (Figure 2-1).

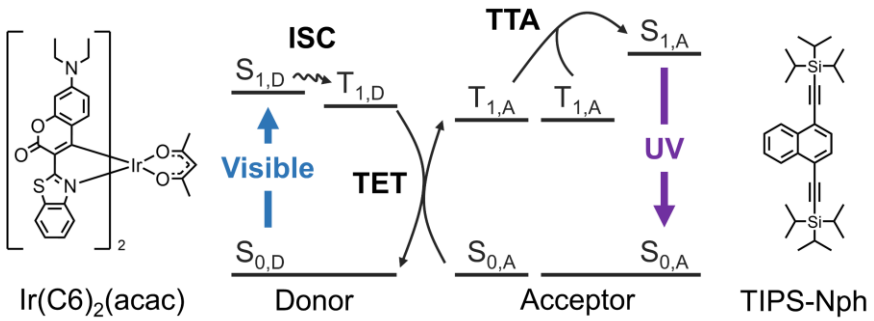

Figure 2-1 Energy diagram of visible-to-UV TTA-UC with $Ir(C6)_2(acac)$ as a donor and TIPS-Nph as an acceptor.

Highly efficient TTA-UC from visible/near-infrared to visible light has been achieved through the outstanding efforts of many research groups.[1-19] On the other hand, the efficiency of TTA-UC (η_{UC}) from visible light ($\lambda > 400$ nm) to UV light ($\lambda < 400$ nm) at solar irradiance has been low.[20-30] The visible-to-UV TTA-UC is very important for photocatalysis and purification of the indoor environment, so it is strongly expected to improve its efficiency. Relatively high η_{UC} of 5.2% and 10.2% for visible-to-UV TTA-UC have been reported using semiconductor nanocrystals as the donor and 2,5-diphenyloxazole (PPO) as the acceptor.[31, 32] However, their threshold excitation intensities (I_{th}) were much higher (ca. 2 W cm^{-2}) than solar irradiance (a few mW cm^{-2}). Lowering the I_{th} value without the decrease in the η_{UC} value is difficult since the broad absorption of conventional donors in the UV region inevitably induces re-absorption and back energy transfer at high donor concentrations.

In order to realize efficient visible-to-UV TTA-UC, it is essential to use a donor with small UV absorption and an acceptor with high fluorescence quantum yield and *f* value. However, the T_1 level of $Ir(C6)_2(acac)$, known as a superior donor with small UV absorption, is 2.19 eV (565 nm),[22] thus

the conventional acceptors such as *p*-terphenyl and 2,5-diphenyloxazole cannot be used. Pyrene is an acceptor that can be combined, but it forms an excimer under high concentration conditions, making it inappropriate for highly efficient TTA-UC systems. Acene derivatives such as anthracene and tetracene are used in the TTA and singlet fission fields (Figure 2-2 and Figure 2-3),[33] and molecules satisfying $2T_1 > S_1$ exhibit TTA activity. In particular, TIPS-anthracene is known as a blue-emitting chromophore.[34, 35] TIPS-anthracene has been reported as an acceptor for TTA-UC, yielding a solution system with an upconversion efficiency of 54% and an estimated *f* value of 77%.[35] To apply these excellent TTA properties to visible-to-UV TTA-UC, we focused on a naphthalene backbone with TIPS groups, which are predicted to have UV emission, low T_1 due to the ethynyl group, and high *f* value similar to TIPS-anthracene.

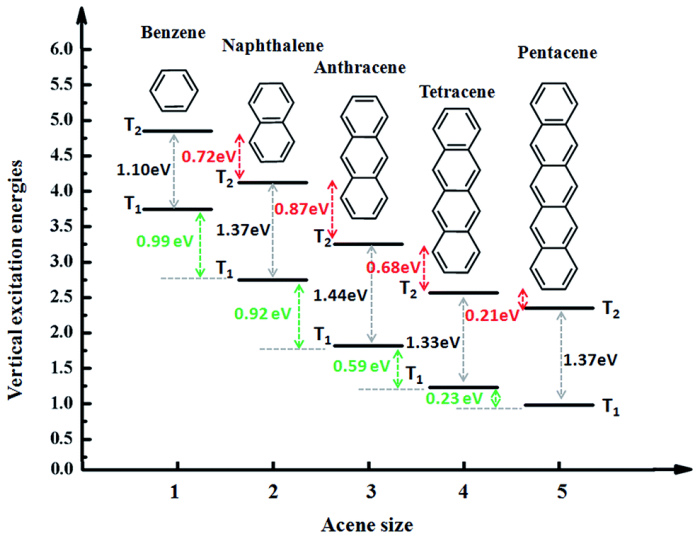

Figure 2-2 Energy diagrams of benzene, naphthalene, anthracene, tetracene, and pentacene. Reproduced with permission from Ref. [33]. Copyright 2017 RSC Publishing.

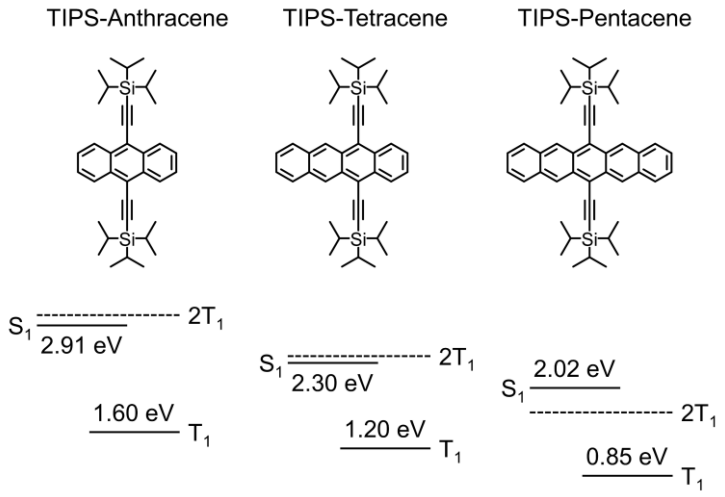

Figure 2-3 Energy diagram of TIPS-anthracene,[35] TIPS-tetracene,[36] and TIPS-pentacene.[37]

This chapter achieves the highest visible-to-UV TTA-UC efficiency η_{UC} of 20.5%, twice as high as the previous record.[31, 32] This new record is made possible by the discovery of a novel superior acceptor 1,4-bis((triisopropylsilyl)ethynyl)naphthalene (TIPS-Nph). Considering that TIPS-tetracene/anthracene are well-studied compounds,[15, 35, 38] it is surprising that TIPS-Nph is not investigated. TIPS-Nph has excellent features as an acceptor and exhibits a high fluorescence quantum yield and a high singlet generation efficiency by the TTA process. Moreover, the triplet energy level of TIPS-Nph is low enough to be sensitized by a donor $Ir(C6)_2(acac)$ (C6 = coumarin 6, acac = acetylacetone).[22] This donor shows strong visible absorption over 80,000 M^{-1} cm^{-1} and weak UV absorption,[22, 39, 40] thus it does not quench upconversion emission in the UV range even at high concentrations. The combination of TIPS-Nph and $Ir(C6)_2(acac)$ also achieves a low I_{th} value below solar intensity. Furthermore, upconverted emission is also observed under a solar simulator and desk LED light.

2-2 Experimental section

2-2-1 General characterization

For synthesis, ^{1}H NMR (400 MHz) and ^{13}C NMR (101 MHz) were measured using a JNM-ECZ-400S (JEOL) instrument using tetramethylsilane (TMS) as an internal standard. Elemental analysis was performed using a CHN Corder MT-5 (Yanaco) at the Elemental Analysis Center, Kyushu University.

For photophysical properties, absorption spectra were measured with a V-780 (JASCO), and photoluminescence spectra were obtained using FP-8300 and FP-8700 (JASCO). Absolute quantum yields of fluorescence and phosphorescence were measured with an integrating sphere connected to a multichannel analyzer C10027-01 (Hamamatsu Photonics). Time-resolved photoluminescence lifetime measurements were performed using a time-correlated single-photon counting (TCSPC) lifetime system Quantaurus-Tau C11367-02 and C11567-01 (Hamamatsu Photonics).

For TTA-UC measurements, a diode laser with a wavelength of 445 nm (75 mW, RGB Photonics) was used as an excitation light source. A software (Ltune) and a rotatable variable neutral density filter were used to control the laser power. The laser power was monitored by a PD300-UV photodiode sensor (Ophir Photonics), and the diameters of the laser beam ($1/e^2$) were measured at the sample position using a CCD beam profiler SP620 (Ophir Photonics). A typical beam spot was estimated to be 3.5×10^{-4} cm^2 from the beam diameter. The laser beam was focused onto a sample using a lens, and achromatic lenses focused the emitted light from the sample to an optical fiber connected to a multichannel detector MCPD-9800 (Otsuka Electronics). The detector was calibrated using a standard lamp HL-3 plus-CAL (Ocean Optics). Short-pass and long-pass filters were not used between the sample and the detector in the measurements. A portable solar simulator PEC-L01 (Peccell) was used to obtain a simulated AM1.5G solar light. Z-10SL (YAMADA SHOMEI LIGHTING) was used as a desk LED light source. Under the solar simulator and the desk LED light, emission spectra were recorded by a multichannel analyzer C10027-01 (Hamamatsu Photonics).

To measure absolute UC efficiency, a Quantaurus-QY Plus C13534-01 (Hamamatsu Photonics) connected to an integrating sphere,[41] and a 445 nm diode laser (75 mW, RGB Photonics) were used. The scattered and emitted light was monitored by a multichannel analyzer through a 410 nm short-pass filter. The spectrometer, including the integrating sphere and the filter, was calibrated by Hamamatsu Photonics. The calibration of the measurement system was confirmed by measuring the fluorescence quantum yield of coumarin 153 in deaerated ethanol excited at a wavelength of 423 nm using a Xe lamp. The quantum yield of 54.3% was obtained, similar to the values of the literature (53%,[42] 54.6%[43]). Using a deaerated THF solution of TIPS-Nph (10 mM) and $Ir(C6)_2(acac)$ (100 μM) at an excitation intensity of 1.3 W cm^{-2}, the error in the calibration including the short-pass filter was confirmed to be small (< 3%) with and without the filter.

2-2-2 Determination of UC efficiency

2-2-2-1 Relative method

Relative UC efficiencies (η_{UC}) were calculated from the following equation using coumarin 6 in a deaerated THF as a standard.[2, 41] Note that the theoretical maximum value of η_{UC} is standardized to 100%.[44]

$$\eta_{UC} = 2\Phi_{std}\left(\frac{1-10^{-A}_{std}}{1-10^{-A}_{UC}}\right)\left(\frac{E_{UC}}{E_{std}}\right)\left(\frac{I_{std}}{I_{UC}}\right)\left(\frac{n_{UC}}{n_{std}}\right)^2 \quad \text{(Eq. 2-1)}$$

In the equation, Φ, A, E, I, and n represent quantum yield, absorbance at a laser wavelength, integrated photoluminescence spectral profile, excitation intensity, and refractive index of the solvent, respectively. The subscripts UC and std indicate parameters for upconversion and standard systems.

2-2-2-2 Absolute method

An absolute UC efficiency ($\eta_{UC,obs}$) was obtained by the procedure reported by de Mello *et al*.[9, 45] To account for the effects of re-absorption, the observed efficiencies were further corrected using the method Yanai *et al.* reported.[41] Sample solutions were prepared in small volume cuvettes of 1×4×12 mm^3 to minimize the effect of re-absorption.

Measurements were performed using four apparatus and sample configurations: Experiment A, B, C, and D (Figure 2-4). In Experiment (A), a UC sample was placed in an integrating sphere and irradiated with a direct laser beam. Experiment (B) was similar to Experiment (A). However, the integrating sphere was mechanically removed without changing any other configurations. In Experiment (C), the UC sample was placed in the integrating sphere, whose height was higher than the laser beam, and the laser was directed at the wall of the integrating sphere. Experiment (D) was similar to Experiment (A) except that only solvent without chromophores was used as a reference. The subscripts in the following equations denote the type of experimental configurations.

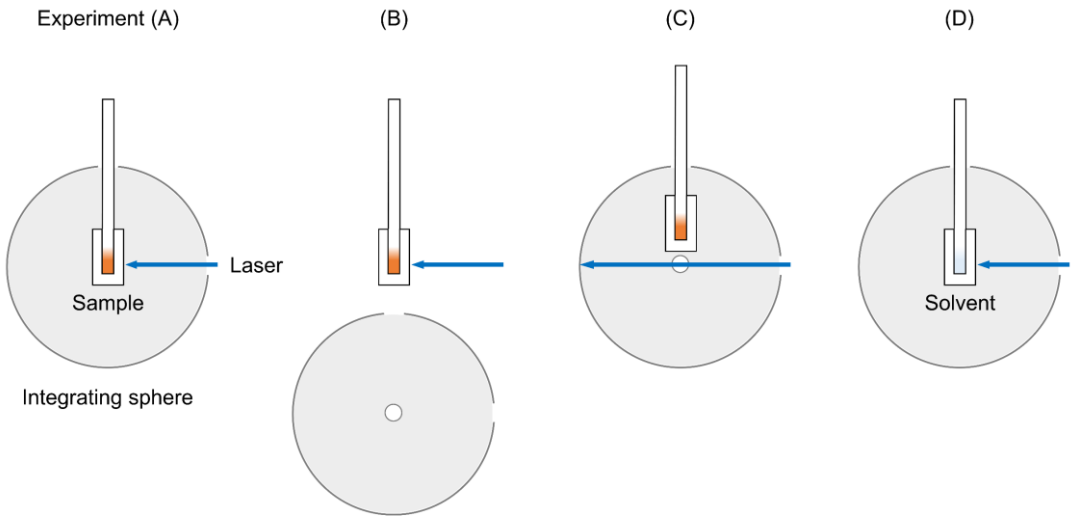

Figure 2-4 Simple illustration of experimental configurations (side view). The detector is on the rear side.

The first-pass absorbance (*Abs*) was estimated by the following equation,

$$Abs = 1 - \frac{L_{\mathrm{A}}}{L_{\mathrm{C}}} \qquad \text{(Eq. 2-2)}$$

where L is the number of laser photons exiting the integrating sphere. The $\eta_{\mathrm{UC,obs}}$ value was estimated by

$$\frac{\eta_{\mathrm{UC,obs}}}{2} = \frac{P_{\mathrm{A}} - (1 - Abs)P_{\mathrm{C}}}{L_{\mathrm{D}}Abs} \qquad \text{(Eq. 2-3)}$$

In the above equation, P is the number of emitted photons. Note that the laser beam was directed to the edge of the sample near the detector to minimize the inner filter effect.[46]

The TTA-UC emission spectra ($P(\lambda)$) in experimental configurations (A) and (B) were normalized at the range of integrated phosphorescence profiles. By using the normalized spectra ($P'(\lambda)$), the re-absorption probability (a) was obtained by the following relationship.

$$\frac{\int_0^\infty P'_{\mathrm{A}}(\lambda)\mathrm{d}\lambda}{\int_0^\infty P'_{\mathrm{B}}(\lambda)\mathrm{d}\lambda} = 1 - a \qquad \text{(Eq. 2-4)}$$

The re-absorption probability was determined by taking the ratio of the integral areas of two normalized TTA-UC emission spectra. Assuming that the re-absorbed photons were approximately lost, the absolute UC efficiency ($\eta_{\mathrm{UC,obs}}$) was obtained by the following equation.

$$\eta_{\mathrm{UC,obs}} \approx \eta_{\mathrm{UC}}(1 - a) \qquad \text{(Eq. 2-5)}$$

2-2-3 DFT calculations

Density functional theory (DFT) and time-dependent DFT (TD-DFT) calculations were performed using the B3LYP exchange-correlation functional implemented in Gaussian 16 software.[47] TIPS-Nph and PPO ground states were optimized using the 6-311+G(d,p) basis. TD-DFT was then performed using the 6-311+G(d,p) basis to obtain excited singlet and triplet states. The triplet structure of TIPS-Nph was optimized in the 6-311+G(d,p) basis set, which was used to calculate the spin density.

2-2-4 Estimation of triplet lifetime

In the lifetime measurements of UC emission decay, the acceptor triplet lifetime is estimated by the known formula,[48]

$$I_{\mathrm{UC}}(t) \propto \exp\left(\frac{-t}{\tau_{\mathrm{UC}}}\right) = \exp\left(\frac{-2t}{\tau_{\mathrm{T}}}\right) \qquad \text{(Eq. 2-6)}$$

where τ_{UC} and τ_{T} indicate the lifetime of the UC and the lifetime of the acceptor triplet, respectively.

2-2-5 Materials

All reagents used in the synthesis were used as received unless otherwise noted. 1,4-Dibromonaphthalene, triisopropylsilylacetylene, triphenylphosphine, and diisopropylamine were purchased from TCI. Tetrahydrofuran (THF, super dehydrated, stabilizer free) was purchased from Wako. Bis(triphenylphosphine)palladium(II) dichloride was purchased from Aldrich. Copper(I) iodide was purchased from Kishida. For photophysical and TTA-UC measurements, the deaerated solutions were prepared inside an argon-filled glovebox ([O_2] < 0.1 ppm). THF (deoxidized, stabilizer-free) was purchased from Wako. 2-Methyltetrahydrofuran (BHT as a stabilizer) was purchased from Aldrich and was used as a glassy solvent at low temperatures. 2,5-Diphenyloxazole (PPO) was purchased from TCI. The synthesis and characterization of $Ir(C6)_2(acac)$ are described in the literature.[22]

2-2-5-1 Synthesis of 1,4-bis((triisopropylsilyl)ethynyl)naphthalene (TIPS-Nph)

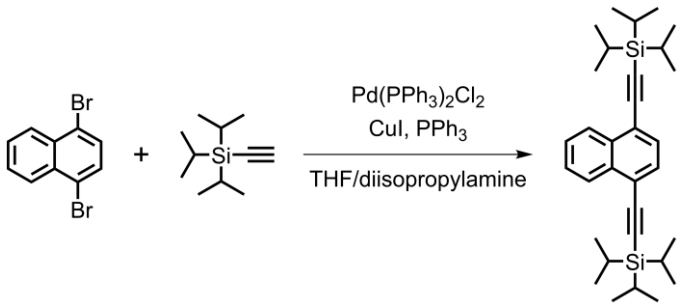

Figure 2-5 Synthesis of TIPS-Nph.

1,4-Dibromonaphthalene (1.44 g, 5.03 mmol), bis(triphenylphosphine)palladium(II) dichloride (80.6 mg, 0.115 mmol), copper(I) iodide (60.4 mg, 0.317 mmol) and triphenylphosphine (82.0 mg, 0.313 mmol) were dissolved in THF (40 mL) under N_2 atmosphere, to which N_2-bubbled diisopropylamine (36 mL) was added. The solution was heated to 100 ℃, and then triisopropylsilylacetylene (3.52 g, 19.3 mmol) was added dropwise, and the resulting solution was stirred at 100 ℃ for 10 hours. After being cooled to room temperature, THF and diisopropylamine were removed under reduced pressure. The residue was extracted with chloroform, dried over anhydrous sodium sulfate, filtered, and dried under reduced pressure. The crude product was purified by silica column chromatography (*n*-hexane) followed by recrystallization from methanol to give TIPS-Nph as a white solid (1.30 g, 53% yield).

^{1}H NMR (400 MHz, $CDCl_3$, TMS): δ (ppm) 8.41-8.38 (m, 2H), 7.63 (s, 2H), 7.61-7.58 (m, 2H), 1.20 (m, 36H), 1.19 (m, 6H)

^{13}C NMR (101 MHz, $CDCl_3$, TMS): δ (ppm) 133.22, 130.14, 127.17, 126.63, 121.79, 104.77, 97.79, 18.77, 11.41

Elemental analysis for $C_{32}H_{48}Si_2$: calculated (%) C 78.61 H 9.90; found (%) C 78.63 H 9.94

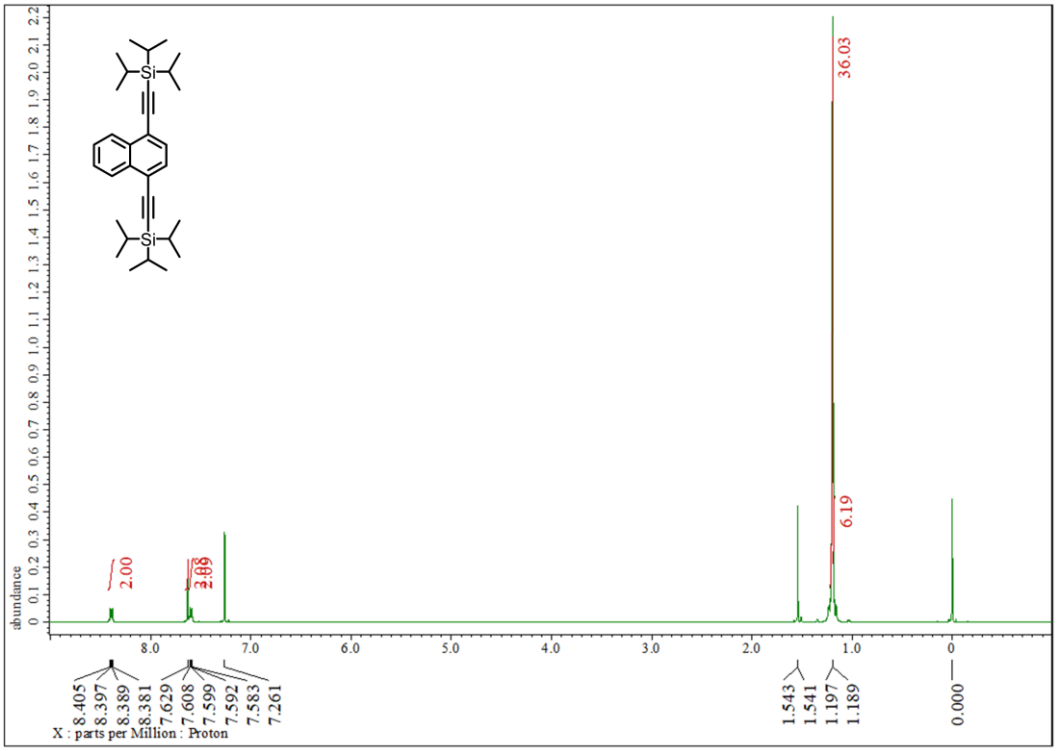

Figure 2-6 ^{1}H NMR of TIPS-Nph (400 MHz, $CDCl_3$, TMS).

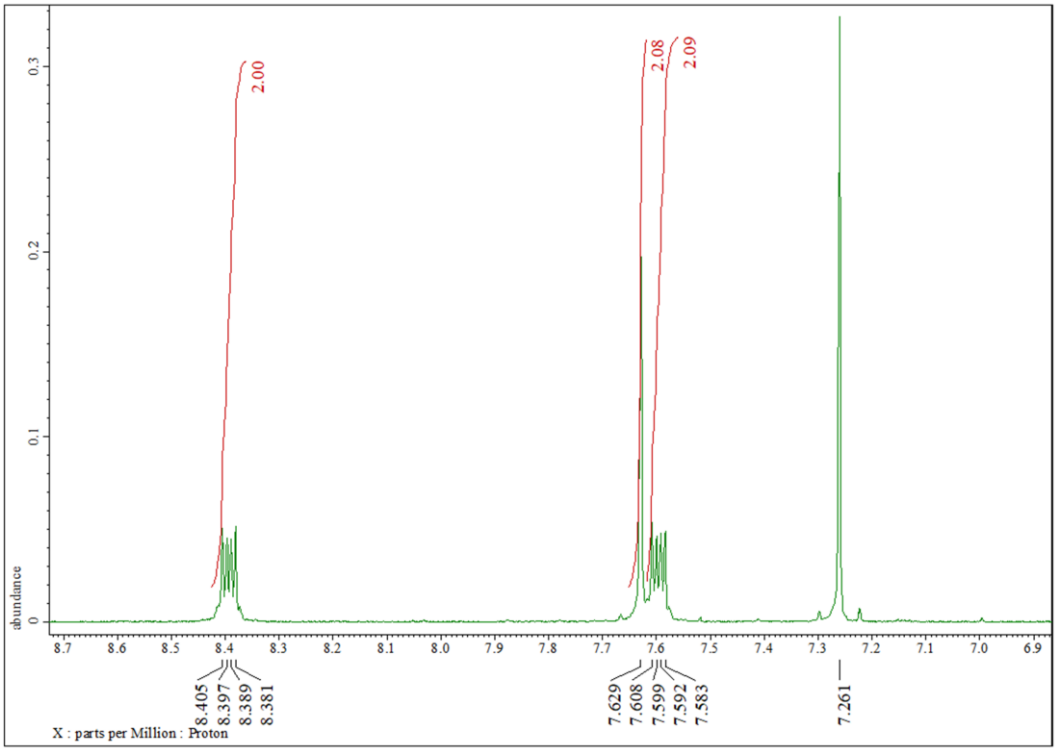

Figure 2-7 Zoomed ^{1}H NMR of TIPS-Nph (400 MHz, $CDCl_3$, TMS).

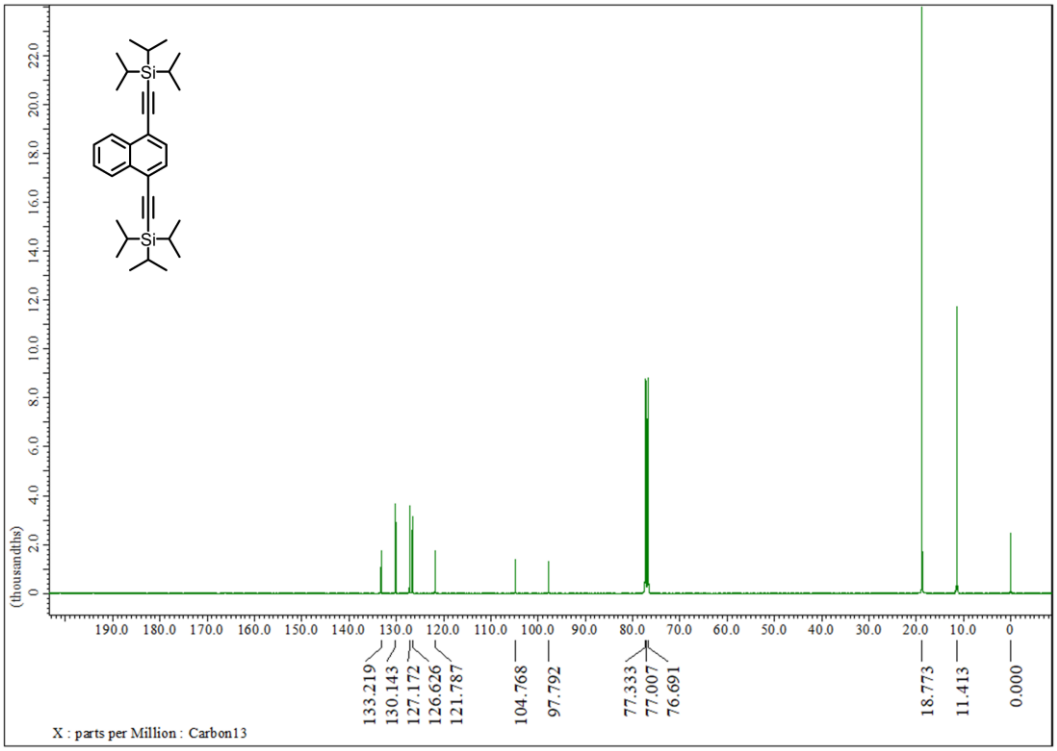

Figure 2-8 ^{13}C NMR of TIPS-Nph (101 MHz, $CDCl_3$, TMS).

2-3 Results and discussion

2-3-1 Synthesis of TIPS-Nph

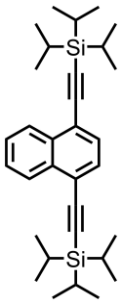

Figure 2-9 Chemical structure of TIPS-Nph.

As a new acceptor in the visible-to-UV TTA-UC, TIPS-Nph was synthesized by Sonogashira coupling reaction of 1,4-dibromonaphthalene with triisopropylsilylacetylene (see 2-2-5-1). TIPS-Nph was obtained as a white solid with high crystallinity and fully characterized by ^{1}H NMR, ^{13}C NMR, and elemental analysis.

2-3-2 DFT calculation of TIPS-Nph

DFT calculation was performed to investigate the electronic states and the energy levels of TIPS-Nph by Gaussian 16 software (see 2-2-3).

The results of the DFT calculations show no significant differences in the optimized structures in the ground and triplet states (Figure 2-10a). The HOMO and LUMO are mainly localized in the naphthalene moiety and are not expected to be affected by the TIPS group (Figure 2-10b). Similarly, the spin density of the triplet state is also localized in the naphthalene moiety, suggesting that the naphthalene moiety dominates the photophysical and TTA properties (Figure 2-10c). The energy levels of TIPS-Nph were then calculated by the TD-DFT method. The S_1 and T_1 levels of TIPS-Nph are 3.44 eV (361 nm) and 2.10 eV (589 nm), respectively. In particular, the T_1 level is lower than that of conventional acceptors, and TIPS-Nph can be combined with a wide variety of donors, including $Ir(C6)_2(acac)$.

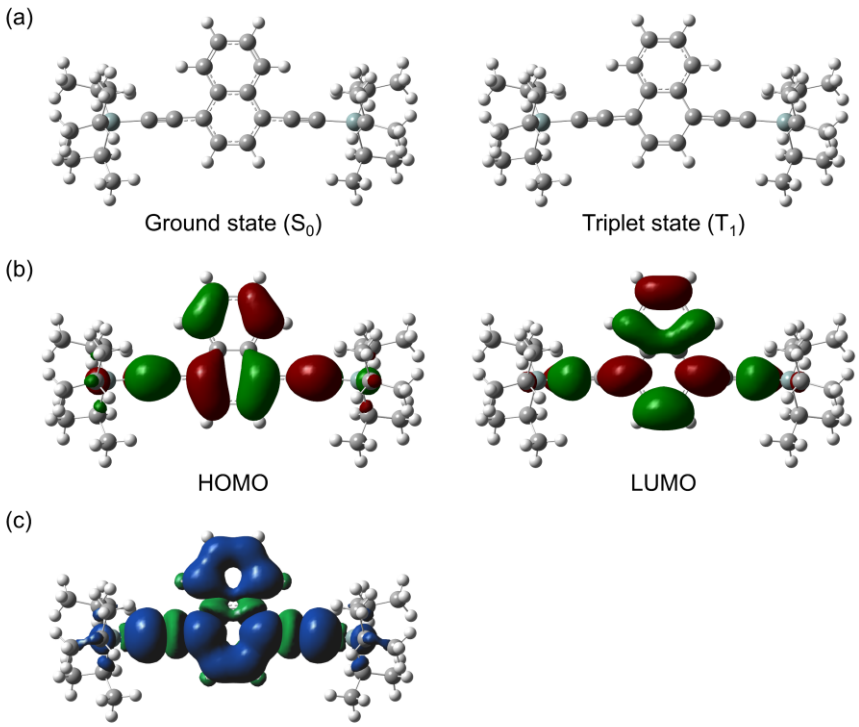

Figure 2-10 (a) Optimized structures of the ground state (S_0) and triplet state (T_1) of TIPS-Nph. (b) HOMO and LUMO orbitals in the ground state (isovalue = 0.02). (c) Spin density surfaces for the triplet state of TIPS-Nph (isovalue = 0.0004).

2-3-3 Photophysical properties of TIPS-Nph

To measure the photophysical properties of TIPS-Nph, a deaerated THF solution of TIPS-Nph was prepared with a concentration of 100 μM. The absorption spectrum of the solution showed a maximum absorption peak at 350 nm (3.54 eV), corresponding to 0-0 absorption (Figure 2-11). As discussed in the above section (see 2-3-2), the S_1 level of the DFT calculation was 3.44 eV, which is similar to the absorption peak, thus validating the DFT calculation results.

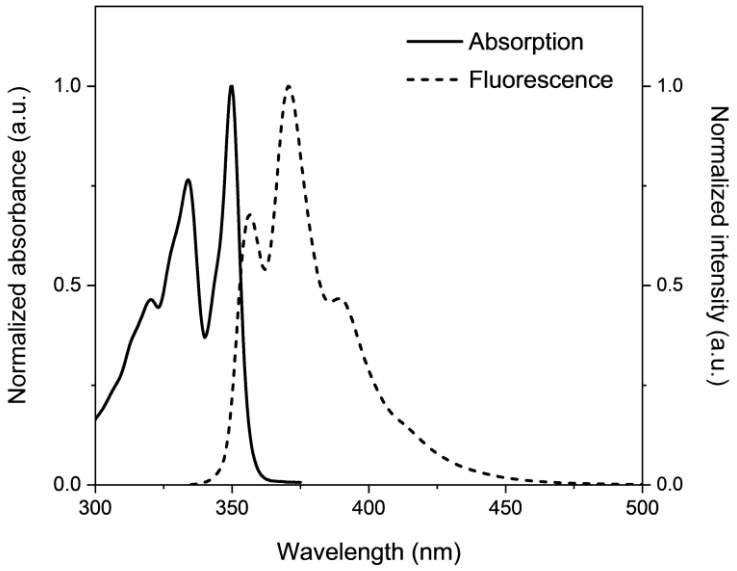

Figure 2-11 Normalized absorption (solid) and fluorescence (dash) spectra of TIPS-Nph ([TIPS-Nph] = 100 μM in deaerated THF).

In the fluorescence spectroscopy, a vibronic spectrum at 357, 371, and 390 nm was observed in the UV region (< 400 nm). Furthermore, a fluorescence quantum yield (Φ_{FL}) of TIPS-Nph determined was relatively high at 74% (λ_{ex} = 320 nm). Since TTA-UC is generally performed under high-concentration conditions, the fluorescence spectrum and quantum yield of TIPS-Nph were measured using a higher-concentration solution ([TIPS-Nph] = 10 mM in deaerated THF). Compared to the lower-concentration solution, the disappearance of the shorter-wavelength peak and the decrease of the fluorescence quantum yield (66%) were observed (Figure 2-12). These changes are ascribed to the inner filter effect by the overlap between the absorption and fluorescence of TIPS-Nph.

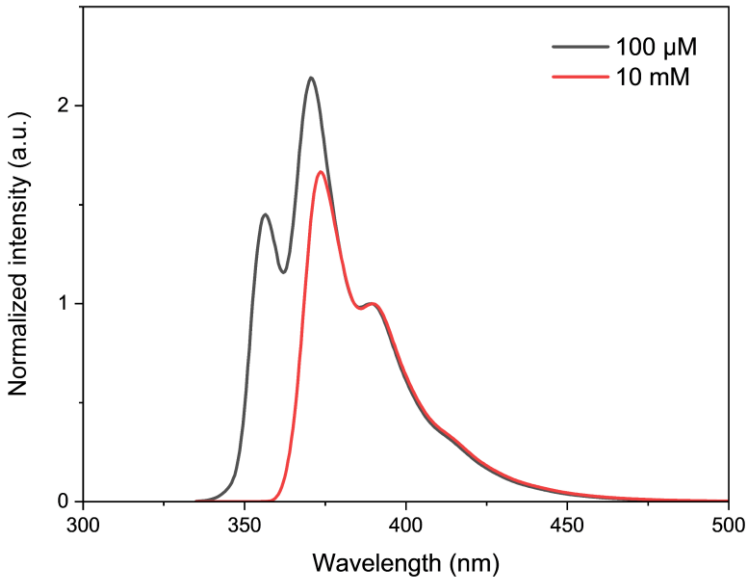

Figure 2-12 Fluorescence spectra of TIPS-Nph normalized at 391 nm (λ_{ex} = 320 nm).

A phosphorescence spectrum was measured using 2-methyltetrahydrofuran at 77 K, and 0-0 emission was observed at 586 nm (2.12 eV), as shown in Figure 2-13, which agrees well with the result of the DFT calculation. The figure also includes the phosphorescence spectrum of PPO, a conventional acceptor, and it is clear that PPO has a shorter-wavelength phosphorescence (524 nm), in other words, a higher T_1 level (2.37 eV).

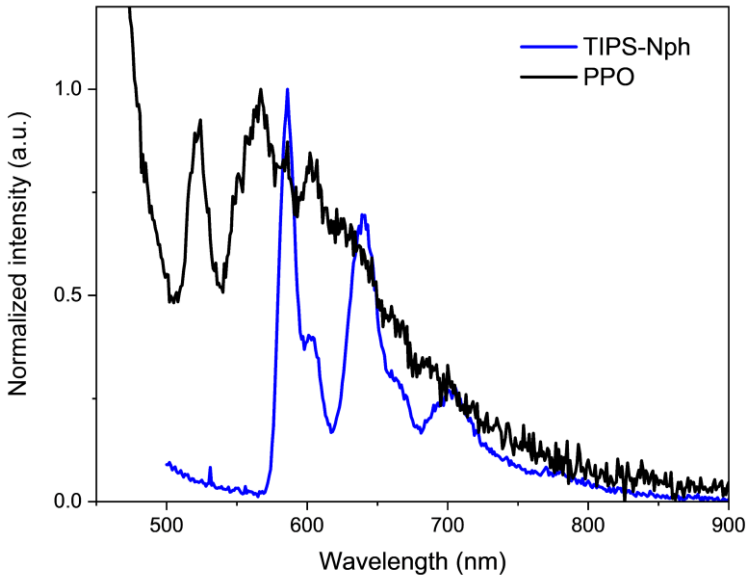

Figure 2-13 Phosphorescence spectra of TIPS-Nph (blue, λ_{ex} = 350 nm) and PPO (black, λ_{ex} = 320 nm) in 2-methyltetrahydrofuran at 77 K ([TIPS-Nph] = 10 mM, [PPO] = 10 mM). The emission of PPO under 500 nm is the tail of fluorescence.

2-3-4 TTA-UC properties of TIPS-Nph paring with Ir(C6)$_2$(acac)

To evaluate TTA-UC, Ir(C6)$_2$(acac) (C6 = coumarin 6, acac = acetylacetone) was selected as the donor (Figure 2-14). Ir(C6)$_2$(acac) exhibits a high absorption band with 445 and 474 nm peaks in the visible region but a low absorption band in the UV region. These properties are due to the sharp and intense ligand-centered π-π* absorption of Ir(C6)$_2$(acac), as reported by Duan and co-workers.[22] Therefore, it is possible to construct a system that efficiently absorbs excitation light and suppresses the re-absorption of UC emission in the UV region. Although Ir(C6)$_2$(acac) is an excellent donor, it shows phosphorescence at 567 nm (2.19 eV). Thus, conventional acceptors with high T_1 levels cannot be used together. However, TIPS-Nph can be sensitized with Ir(C6)$_2$(acac) since it has a lower T_1 level (2.12 eV) than conventional acceptors.

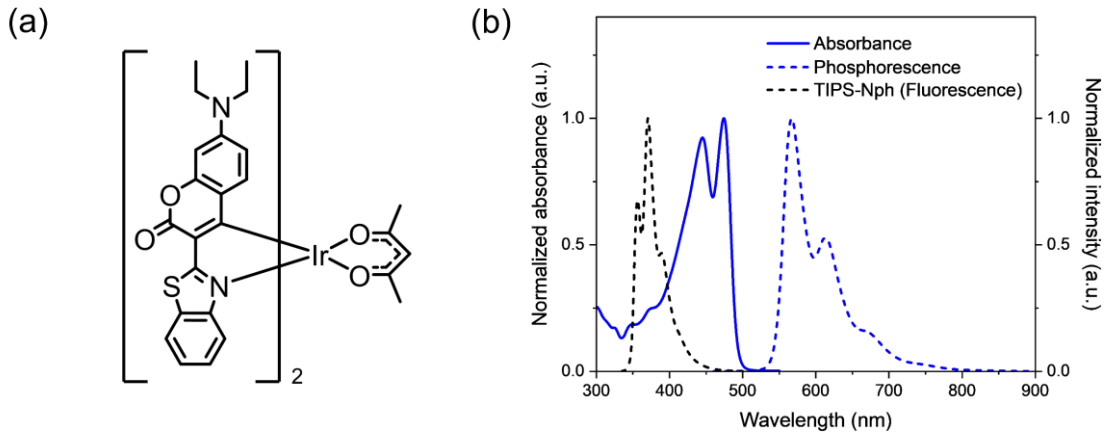

Figure 2-14 (a) Chemical structure of Ir(C6)$_2$(acac). (b) Normalized absorption (blue, solid) and phosphorescence (blue, dash, λ_{ex} = 445 nm) spectra of Ir(C6)$_2$(acac) in deaerated THF ([Ir(C6)$_2$(acac)] = 100 μM). The black dashed line indicates the fluorescence spectrum of TIPS-Nph (same as Figure 2-11).

A deaerated THF solution containing TIPS-Nph and Ir(C6)$_2$(acac) was prepared as a sample for TTA-UC measurement ([TIPS-Nph] = 10 mM, [Ir(C6)$_2$(acac)] = 100 μM). When the THF solution was irradiated with laser light at 445 nm, emission was obtained in the UV range, which is shorter than the excitation light (Figure 2-15a). Lifetime measurements of this emission showed a ms-scale delayed photoluminescence decay, suggesting that this UV emission is attributed to the TTA-UC origin (Figure 2-15b). UC efficiencies (η_{UC}) were then measured by the relative method (see 2-2-2-1), and the maximum UC efficiency was 20.5% (Figure 2-15c). The η_{UC} values are standardized to 100%.[44] Absolute UC efficiency measurements using an integrating sphere were also performed (see 2-2-2-2).[41, 45] The absolute efficiency was corrected using the re-absorption probability (a = 0.51) obtained by taking the ratio of the integrated areas of two normalized TTA-UC emission spectra from 350 to 410 nm (Figure 2-16a, b). The absence of excitation intensity dependence of the re-absorption

probability confirmed that the TTA-UC photoluminescence produced by the re-absorption is negligible (Figure 2-16c). This measurement resulted in a high UC efficiency of 21.4% at 17 W cm^{-2}, supporting the reliability of the relative method.

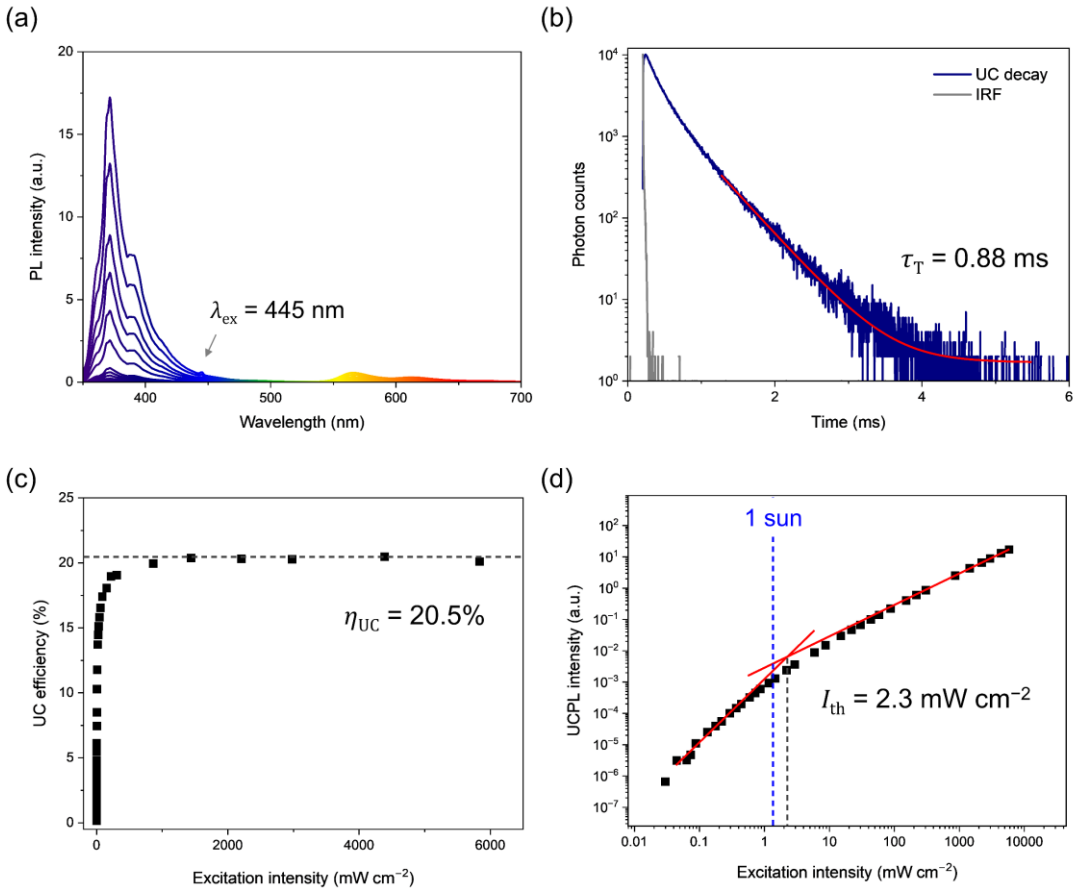

Figure 2-15 (a) Photoluminescence (PL) spectra, (c) UC efficiencies, and (d) UCPL intensities of TIPS-Nph and Ir(C6)$_2$(acac) at various excitation intensities from 0.030 mW cm^{-2} to 5.8 W cm^{-2} (λ_{ex} = 445 nm). (b) UC emission decay monitored at 370 nm under 445 nm excitation light. The gray line shows the instrument response function (IRF). The sample concentrations of TIPS-Nph and Ir(C6)$_2$(acac) were 10 mM and 100 μM in deaerated THF, respectively.

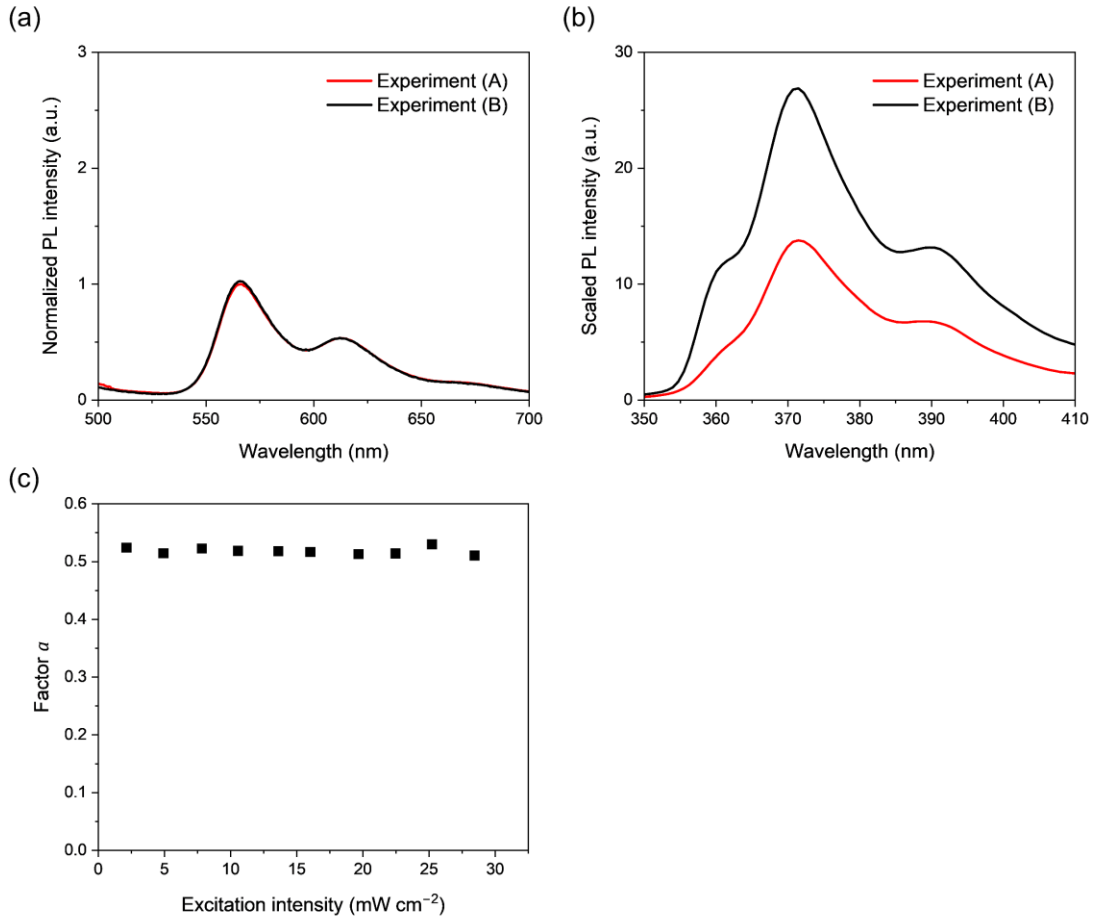

Figure 2-16 (a) Phosphorescence and (b) upconverted emission spectra of the deaerated THF solution containing TIPS-Nph and $Ir(C6)_2(acac)$ under the irradiation with a 445 nm laser at 17 W cm^{-2}. The red and black lines show Experiment (A) and (B) scaled by the integrated phosphorescence profiles from 500 to 700 nm, respectively. (c) Probability of re-absorption (*a*) as a function of excitation intensities varying from 2.1 W cm^{-2} to 28 W cm^{-2}.

The UC efficiency obtained is two times higher than the previously published record of visible-to-UV TTA-UC efficiency (10.2%).[32] In addition to the above experiments, the samples were continuously irradiated by the laser for 1 hour to assess the stability of the UC emission (Figure 2-17). The results showed that the intensity of the UC emission did not change during the irradiation, indicating the high stability of this system. A previous study reported a system using a pyrene derivative as an acceptor with a T_1 level relatively close to that of TIPS-Nph.[22] This system's efficiency was up to 2.0% despite the small re-absorption of UV emission. This may be because pyrene forms excimer under high concentration conditions, and the *f* value is small. In this study, TIPS-Nph showed an efficiency of 20%, which indicates superiority to the conventional acceptor, pyrene. Furthermore, when PPO,[21, 27, 28, 31, 32] a conventional acceptor, was evaluated, the combination of PPO and $Ir(C6)_2(acac)$ did not produce UC emission (Figure 2-18).

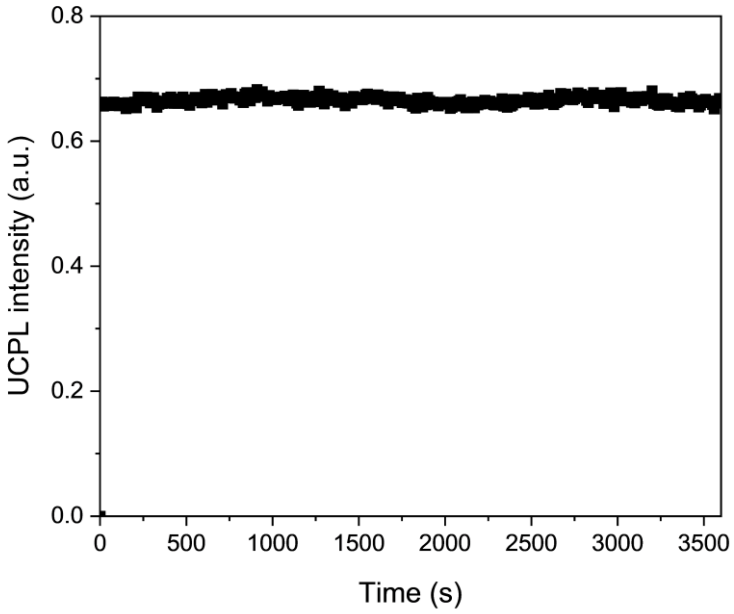

Figure 2-17 PL intensity at 372 nm of TIPS-Nph and $Ir(C6)_2(acac)$ in deaerated THF at 256 mW cm^{-2} for 1 hour.

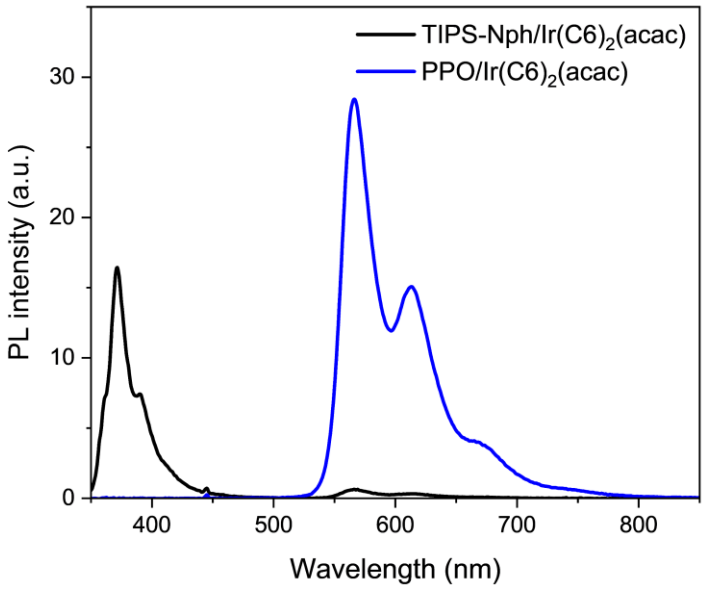

Figure 2-18 PL spectra of TIPS-Nph/$Ir(C6)_2(acac)$ and PPO/$Ir(C6)_2(acac)$ in deaerated THF at 5.5 W cm^{-2} under the 445 nm laser. The concentrations of TIPS-Nph, PPO, and $Ir(C6)_2(acac)$ are 10 mM, 10 mM, and 100 μM, respectively.

The difference in UC emission between TIPS-Nph and PPO can be attributed to the difference in the triplet energy transfer (TET) efficiency (Φ_{TET}) from the donor to the acceptor. The phosphorescence quantum yields of the donors in the UC samples were measured, and Φ_{TET} was calculated using the following equations,

$$\Phi_{TET} = 1 - \frac{\Phi_P}{\Phi_{P,0}} \qquad \text{(Eq. 2-7)}$$

where Φ_P and $\Phi_{P,0}$ represent the quantum yields of phosphorescence of the donor ($Ir(C6)_2(acac)$) with and without the acceptor (TIPS-Nph and PPO). Using the $\Phi_{P,0}$ value of 79% ([$Ir(C6)_2(acac)$] = 100 μM in deaerated THF), Φ_{TET} values were calculated to be 97% for the TIPS-Nph system and almost 0% for the PPO system, respectively. From the DFT calculation and the phosphorescence measurement, it is already known that the T_1 of TIPS-Nph is lower than $Ir(C6)_2(acac)$. On the other hand, the T_1 level of PPO was 2.51 eV by the DFT calculation and 2.37 eV by the phosphorescence measurement at 77 K. Thus, PPO has a higher T_1 level than the donor, which is probably the reason for the difference in the low TET efficiency and the absence of UC emission. These results indicate that TIPS-Nph is a better acceptor than conventional ones and can be combined with $Ir(C6)_2(acac)$, which is useful for constructing efficient TTA-UC systems.

UC efficiency is expressed as the product of the efficiencies of each TTA-UC process and can be

discussed by the following equation.[5]

$$\eta_{UC} = f\Phi_{ISC}\Phi_{TET}\Phi_{TTA}\Phi_{FL} \quad \text{(Eq. 2-8)}$$

In the equation, Φ_{ISC} and Φ_{TTA} are quantum yields of the donor ISC and the TTA, respectively. Because there was no donor fluorescence and the maximum UC efficiency was calculated in the region of high enough excitation intensity discussed later, these parameters are assumed to be approximately 100%. The *f* value is estimated to be 32% by substituting the obtained parameters into the equation. The maximum *f* value calculated from the typical spin statistics is 40%, indicating that the present result is relatively high and why this system showed record-breaking UC efficiency. The reason for the high *f* value is not entirely apparent. Rao and co-workers have reported that the rigid bonding of ethynyl groups suppresses nonradiative losses during the TTA process,[35] which may be involved in the present case. Therefore, screening naphthalene structures with ethynyl groups for TTA-UC properties should provide more efficient acceptor molecules in the future.

In addition to UC efficiency, the threshold excitation intensity (I_{th}) is critical to evaluate the properties of TTA-UC. In typical TTA-UC systems, the dependence of the UC emission intensity is quadratic to linear on the excitation intensity in low- and high-intensity regimes, respectively.[49-51] The intersection of the UC emission intensity fitting lines, displayed in the log-log plot, is the threshold excitation intensity. In this system of TIPS-Nph (10 mM) and $Ir(C6)_2(acac)$ (100 μM), the slope of the fitting line varies from 2.0 to 1.0 with excitation intensity, which is consistent with typical characteristics of TTA-UC systems (Figure 2-15d). The I_{th} calculated from these slopes was 2.3 mW cm^{-2}. Surprisingly, when the donor concentration was changed from 100 μM to 300 μM, the I_{th} value dropped to 1.1 mW cm^{-2} with slopes from 2.0 to 1.0, which is lower than the solar irradiance of 1.4 mW cm^{-2} for 445 ± 5 nm (Figure 2-19d).

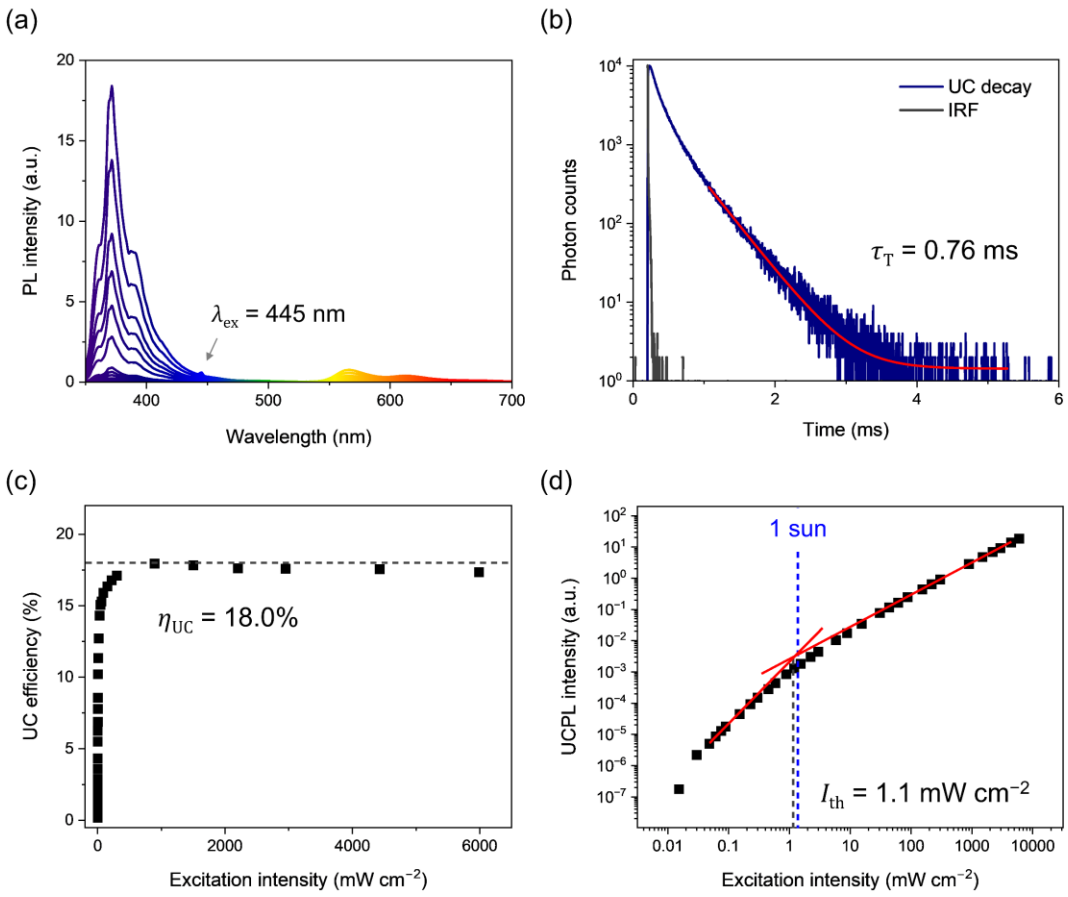

Figure 2-19 (a) PL spectra, (c) UC efficiencies, and (d) UCPL intensities of TIPS-Nph and $Ir(C6)_2(acac)$ at various excitation intensities from 0.015 mW cm^{-2} to 6.0 W cm^{-2} (λ_{ex} = 445 nm). (b) UC emission decay monitored at 370 nm under 445 nm excitation light. The gray line shows the instrument response function (IRF). The TIPS-Nph and $Ir(C6)_2(acac)$ sample concentrations were 10 mM and 300 μM in deaerated THF, respectively.

2-3-5 Evaluation of internal and external UC efficiency

Although the internal UC efficiency (η_{UC}) discussed above (see 2-3-4) is commonly used to evaluate basic TTA-UC properties, in practical applications, it is important to consider the external UC efficiency ($\eta_{UC,ext}$) that also considers donors' absorption. The following equation defines it.

$$\eta_{UC,ext} = \eta_{UC}(1 - 10^{-A}) \qquad \text{(Eq. 2-9)}$$

In the equation, A represents the absorbance of the donor at the excitation wavelength. Applying this equation to the system of TIPS-Nph and Ir(C6)$_2$(acac), a high efficiency of 17.4% was obtained at a donor concentration of 300 μM (Figure 2-20). Furthermore, the external UC efficiency was about 6%, even at a solar intensity of 1.4 mW cm^{-2}.

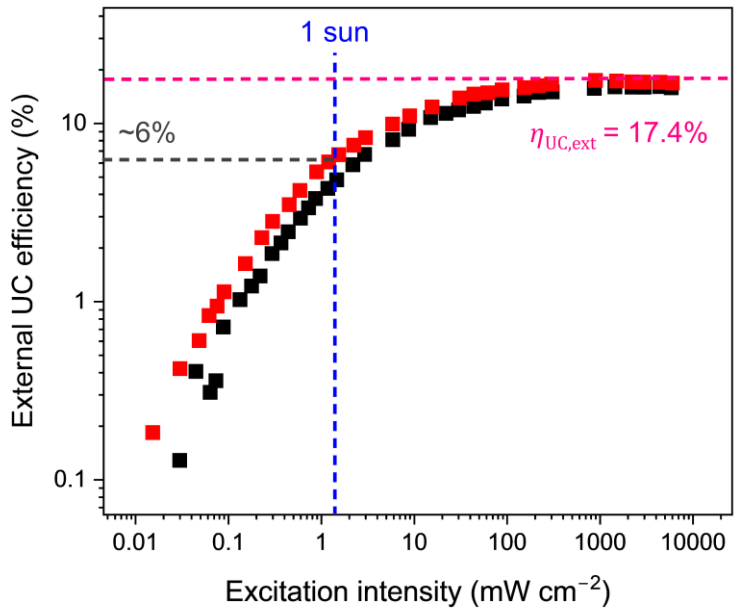

Figure 2-20 External UC efficiency of the deaerated THF solutions containing TIPS-Nph (10 mM) and Ir(C6)$_2$(acac) with different concentrations of 100 μM (black) and 300 μM (red). The blue dashed line indicates the intensity of sunlight (1.4 mW cm^{-2} for 445 ± 5nm).

TTA-UC properties are usually evaluated at low donor concentrations (low absorbance) because high donor concentrations can cause re-absorption and back energy transfer of UC emission, leading to lower UC efficiency. In this case, efficient $\eta_{UC,ext}$ is not achieved even if η_{UC} is high. On the other hand, this system can perform high η_{UC} even under high donor absorbance conditions due to the excellent absorption properties of Ir(C6)$_2$(acac) and its high absorption in the visible and low in the UV region (Figure 2-19a, c). That is why high external UC efficiency was achieved and is a notable feature of the current system. At the high donor concentration, 97% of the light was absorbed at 445nm (A = 1.55, optical path length = 1 mm), while at the same time, an internal UC efficiency of 18.0%

was achieved. In addition, the UV absorption of the donor is weak in this system, and the T_1 of the acceptor is lower than that of the donor, which suppresses the singlet and triplet energy transfer, respectively. These were confirmed by the fact that the fluorescence lifetime of the acceptor with and without the donor was comparable (Figure 2-21) and that the triplet lifetime was similar at different donor concentrations (Figure 2-15b and Figure 2-19b).

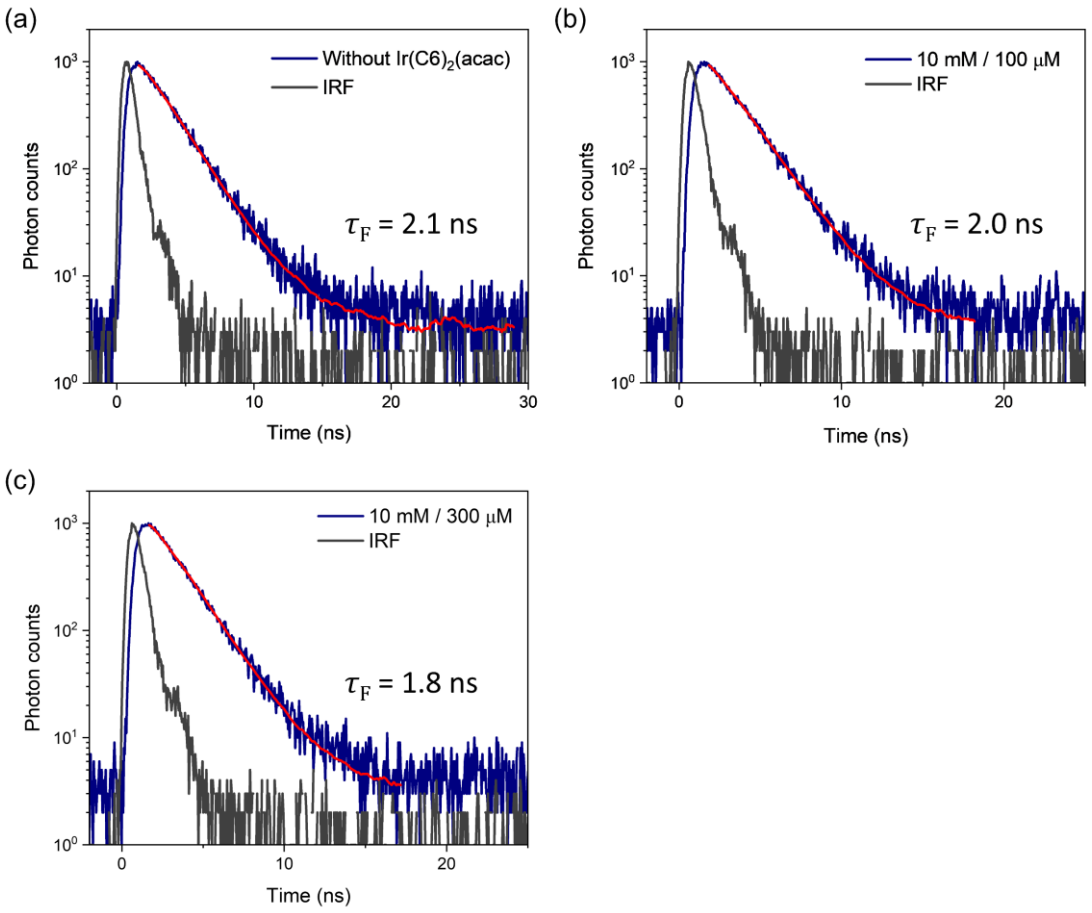

Figure 2-21 Fluorescence decays of TIPS-Nph (10 mM) without (a) and with (b, c) $Ir(C6)_2(acac)$ at 370 nm under the excitation light of 340 nm. Concentrations of $Ir(C6)_2(acac)$ were (b) 100 μM and (c) 300 μM, respectively.

2-3-6 Demonstration of TTA-UC under solar simulator and LED light

A simple demonstration of the combination of TIPS-Nph and $Ir(C6)_2(acac)$ was performed using a solar simulator. A deaerated THF solution was used as a sample, and a 450 nm long-pass filter was inserted into the solar simulator to avoid direct excitation of TIPS-Nph. Under 1sun condition and without focusing the excitation light, emission was obtained in the UV region (Figure 2-22). Since no emission was obtained when the sample without the donor was measured, it was confirmed that the obtained UV emission was generated from TTA-UC. A photocatalyst with a quantum yield of almost 100% for water splitting has been reported, but the absorption of the photocatalyst has been limited to the UV range.[52] The visible-to-UV TTA-UC is anticipated to provide visible light sensitivity to the photocatalyst. Since some photocatalysts require UV light below 360 nm, tuning the emission wavelength of the TTA-UC is necessary.

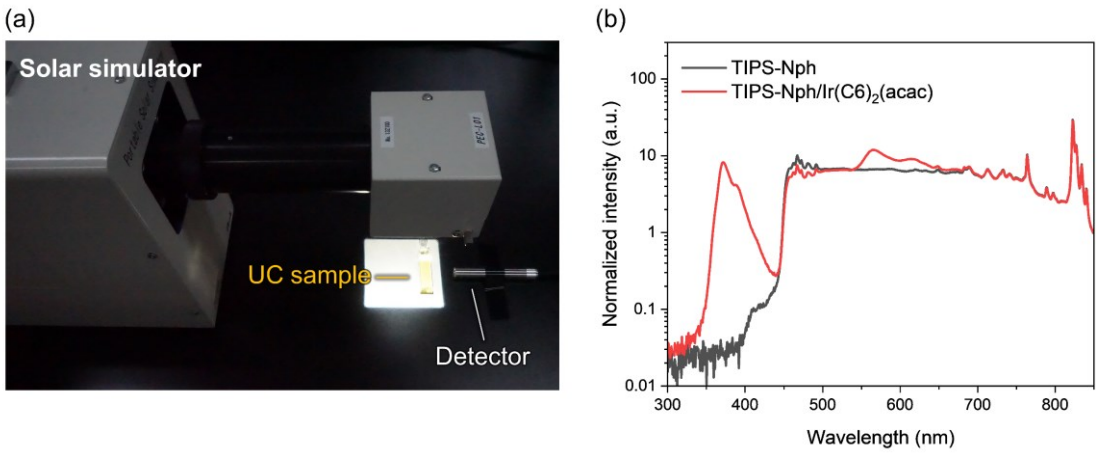

Figure 2-22 (a) A photograph of the setup using a solar simulator in which a 450 nm long-pass filter is included. (b) PL spectra (normalized at 850 nm) of TIPS-Nph with (red) and without (gray) $Ir(C6)_2(acac)$ in deaerated THF ([TIPS-Nph] = 10 mM, $[Ir(C6)_2(acac)]$ = 100 μM).

The most important application of visible-to-UV TTA-UC is the effective use of indoor light, which is weaker than sunlight. Therefore, desk LED light with an intensity of about 0.7 mW cm^{-2} in the blue portion (λ < 500 nm) was used to test the TTA-UC system. The sample and LED surfaces were about 7 cm apart. As a result, the THF solution of TIPS-Nph and $Ir(C6)_2(acac)$ showed clear UV emission even when the intensity of the excitation light of the LED light was weak (Figure 2-23). When measurements were performed without the donor, no emission was observed in the UV region, indicating that the obtained emission was derived from TTA-UC. The distance between the LED and the sample was then varied from 5 cm to 50 cm, and the light intensity of the LED (λ < 500 nm) was varied from 0.88 mW cm^{-2} to 0.065 mW cm^{-2} (Figure 2-24). Surprisingly, the TTA-UC system showed UC emission even when the LED light was 50 cm away. By formulating a solid-state upconverter based on the current donor-acceptor dye and combining it with photocatalysts, TTA-UC would

contribute to purifying indoor environments.

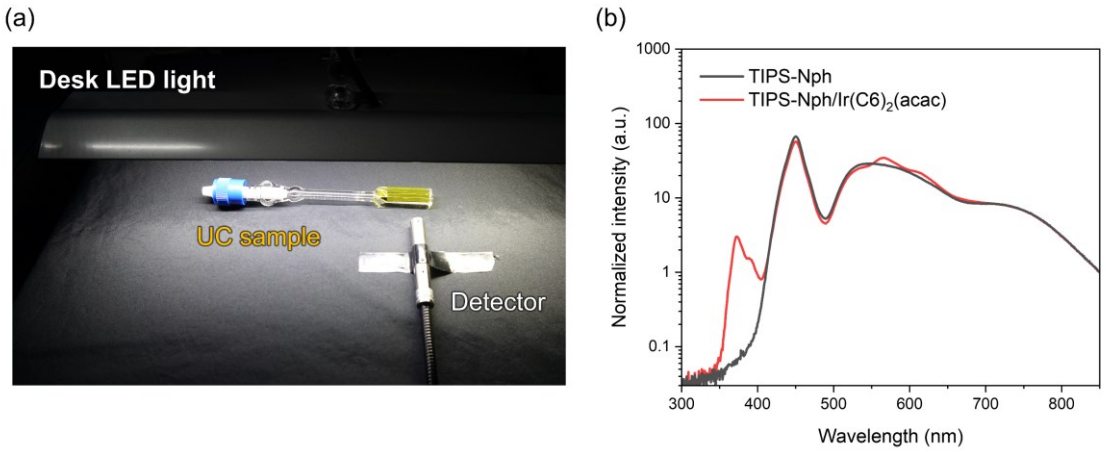

Figure 2-23 (a) A photograph of the setup using a desk LED light at about 0.7 mW cm^{-2} (λ < 500 nm) without using any lenses and filters. (b) PL spectra (normalized at 850 nm) of TIPS-Nph with (red) and without (gray) $Ir(C6)_2(acac)$ in deaerated THF ([TIPS-Nph] = 10 mM, [$Ir(C6)_2(acac)$] = 100 μM).

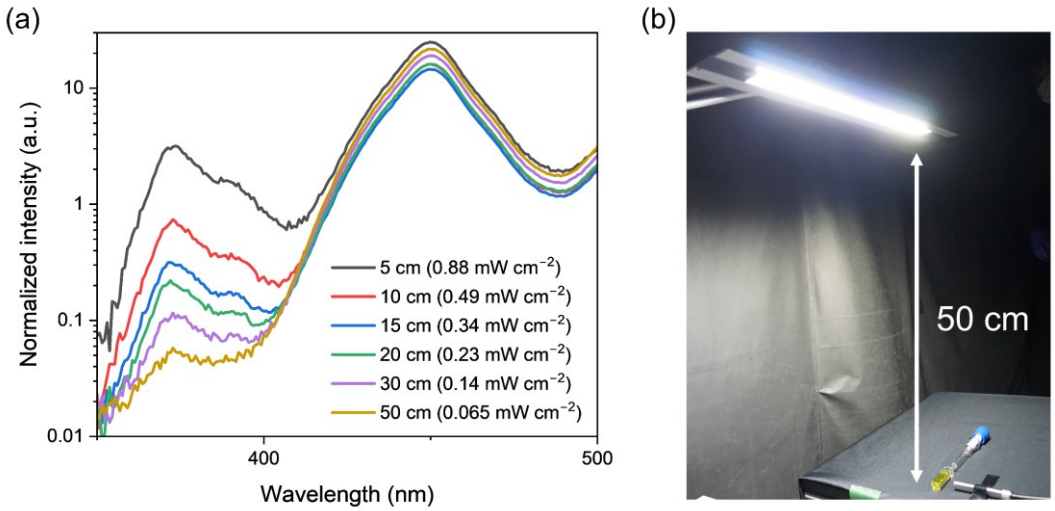

Figure 2-24 (a) Photoluminescence spectra of a deaerated THF solution containing TIPS-Nph and $Ir(C6)_2(acac)$ at different distances from the LED light ([TIPS-Nph] = 10 mM, $[Ir(C6)_2(acac)]$ = 100 μM). LED light intensities are calculated below 500 nm. (b) A photograph of the measurement setup with the desk LED light at a distance of 50 cm.

2-4 Conclusion

In conclusion, this work shows the highest visible-to-UV TTA-UC efficiency (η_{UC}) of 20.5%, two times higher than the previous record. The highest UC efficiency was certified by the absolute photoluminescence quantum yield method. This breakthrough in UC efficiency was achieved by discovering the excellent UV-emitting acceptor TIPS-Nph, which exhibits a high fluorescence quantum yield and *f* value. TIPS-Nph has a lower triplet level than the excellent donor $Ir(C6)_2(acac)$, and this donor-acceptor combination yields a threshold excitation intensity (I_{th}) of 1.1 mW cm^{-2}, which is lower than the solar intensity. Although it is usually challenging to realize the high external UC efficiency ($\eta_{UC,ext}$) due to the significant quenching of UC emission at high donor concentrations, the donor's large visible absorption and small UV absorption characteristics result in an external UC efficiency of 17.4%. Even weak visible light, such as sunlight and LED light, can be efficiently converted to UV light, showing the promising potential for various outdoor and indoor applications.

2-5 References

[1] S. Baluschev, T. Miteva, V. Yakutkin, G. Nelles, A. Yasuda and G. Wegner, *Phys. Rev. Lett.*, 2006, **97**, 143903.

[2] T. N. Singh-Rachford and F. N. Castellano, *Coord. Chem. Rev.*, 2010, **254**, 2560-2573.

[3] J. Zhao, S. Ji and H. Guo, *RSC Adv.*, 2011, **1**, 937-950.

[4] J.-H. Kim and J.-H. Kim, *J. Am. Chem. Soc.*, 2012, **134**, 17478-17481.

[5] A. Monguzzi, R. Tubino, S. Hoseinkhani, M. Campione and F. Meinardi, *Phys Chem Chem Phys*, 2012, **14**, 4322-4332.

[6] Y. C. Simon and C. Weder, *J. Mater. Chem.*, 2012, **22**, 20817-20830.

[7] V. Gray, D. Dzebo, M. Abrahamsson, B. Albinsson and K. Moth-Poulsen, *Phys. Chem. Chem. Phys.*, 2014, **16**, 10345-10352.

[8] R. Andernach, H. Utzat, S. D. Dimitrov, I. McCulloch, M. Heeney, J. R. Durrant and H. Bronstein, *J. Am. Chem. Soc.*, 2015, **137**, 10383-10390.

[9] M. Wu, D. N. Congreve, M. W. B. Wilson, J. Jean, N. Geva, M. Welborn, T. Van Voorhis, V. Bulović, M. G. Bawendi and M. A. Baldo, *Nat. Photon.*, 2016, **10**, 31-34.

[10] S. P. Hill and K. Hanson, *J. Am. Chem. Soc.*, 2017, **139**, 10988-10991.

[11] Z. Huang and M. L. Tang, *J. Am. Chem. Soc.*, 2017, **139**, 9412-9418.

[12] N. Yanai and N. Kimizuka, *Acc. Chem. Res.*, 2017, **50**, 2487-2495.

[13] J. M. Rowe, J. Zhu, E. M. Soderstrom, W. Xu, A. Yakovenko and A. J. Morris, *Chem. Commun.*, 2018, **54**, 7798-7801.

[14] R. Sato, H. Kitoh-Nishioka, K. Kamada, T. Mizokuro, K. Kobayashi and Y. Shigeta, *J. Phys. Chem. Lett.*, 2018, **9**, 6638-6643.

[15] C. J. Imperiale, P. B. Green, E. G. Miller, N. H. Damrauer and M. W. B. Wilson, *J. Phys. Chem. Lett.*, 2019, **10**, 7463-7469.

[16] B. D. Ravetz, A. B. Pun, E. M. Churchill, D. N. Congreve, T. Rovis and L. M. Campos, *Nature*, 2019, **565**, 343-346.

[17] S. Wieghold, A. S. Bieber, Z. A. VanOrman, L. Daley, M. Leger, J.-P. Correa-Baena and L. Nienhaus, *Matter*, 2019, **1**, 705-719.

[18] X. Yang, J. Han, Y. Wang and P. Duan, *Chem. Sci.*, 2019, **10**, 172-178.

[19] E. M. Gholizadeh, S. K. K. Prasad, Z. L. Teh, T. Ishwara, S. Norman, A. J. Petty II, J. H. Cole, S. Cheong, R. D. Tilley, J. E. Anthony, S. Huang and T. W. Schmidt, *Nat. Photon.*, 2020, **14**, 585-590.

[20] W. Zhao and F. N. Castellano, *J. Phys. Chem. A*, 2006, **110**, 11440-11445.

[21] T. N. Singh-Rachford and F. N. Castellano, *J. Phys. Chem. A*, 2009, **113**, 5912-5917.

[22] P. Duan, N. Yanai and N. Kimizuka, *Chem. Commun.*, 2014, **50**, 13111-13113.

[23] X. Jiang, X. Guo, J. Peng, D. Zhao and Y. Ma, *ACS Appl. Mater. Interfaces*, 2016, **8**, 11441-11449.

[24] J. Peng, X. Guo, X. Jiang, D. Zhao and Y. Ma, *Chem. Sci.*, 2016, **7**, 1233-1237.

[25] N. Yanai, M. Kozue, S. Amemori, R. Kabe, C. Adachi and N. Kimizuka, *J. Mater. Chem. C*, 2016, **4**, 6447-6451.

[26] Q. Chen, Y. Liu, X. Guo, J. Peng, S. Garakyaraghi, C. M. Papa, F. N. Castellano, D. Zhao and Y. Ma, *J. Phys. Chem. A*, 2018, **122**, 6673-6682.

[27] K. Okumura, N. Yanai and N. Kimizuka, *Chem. Lett.*, 2019, **48**, 1347-1350.

[28] S. Hisamitsu, J. Miyano, K. Okumura, J. K.-H. Hui, N. Yanai and N. Kimizuka, *ChemistryOpen*, 2020, **9**, 14-17.

[29] Y. Kawashima, H. Kouno, K. Orihashi, K. Nishimura, N. Yanai and N. Kimizuka, *Mol. Syst. Des. Eng.*, 2020, **5**, 792-796.

[30] B. Pfund, D. M. Steffen, M. R. Schreier, M. S. Bertrams, C. Ye, K. Börjesson, O. S. Wenger and C. Kerzig, *J. Am. Chem. Soc.*, 2020, **142**, 10468-10476.

[31] V. Gray, P. Xia, Z. Huang, E. Moses, A. Fast, D. A. Fishman, V. I. Vullev, M. Abrahamsson, K. Moth-Poulsen and M. L. Tang, *Chem. Sci.*, 2017, **8**, 5488-5496.

[32] S. He, X. Luo, X. Liu, Y. Li and K. Wu, *J. Phys. Chem. Lett.*, 2019, **10**, 5036-5040.

[33] Y. Y. Pan, J. Huang, Z, D. W. Yu, B. Yang and Y. G. Ma, *RSC Adv.*, 2017, **7**, 26697-26703.

[34] T. W. Schmidt, R. W. MacQueen, C. B. Dover, S. K. K. Prasad, L. Frazer, J. K. Gallaher and J. K. H. Pun, *J. Photon. Energy*, 2018, **8**, 022006.

[35] N. Nishimura, V. Gray, J. R. Allardice, Z. Zhang, A. Pershin, D. Beljonne and A. Rao, *ACS Mater. Lett.*, 2019, **1**, 660-664.

[36] N. Alagna, J. Han, N. Wollscheid, J. L. Perez Lustres, J. Herz, S. Hahn, S. Koser, F. Paulus, U. H. F. Bunz, A. Dreuw, T. Buckup and M. Motzkus, *J. Am. Chem. Soc.*, 2019, **141**, 8834-8845.

[37] N. Wollscheid, J. L. Pérez Lustres, O. Kefer, S. Hahn, V. Brosius, U. H. F. Bunz, M. Motzkus and T. Buckup, *Nat. Commun.*, 2019, **10**.

[38] A. B. Pun, Samuel, M. Y. Sfeir, L. M. Campos and D. N. Congreve, *Chem. Sci.*, 2019, **10**, 3969-3975.

[39] S. Lamansky, P. Djurovich, D. Murphy, F. Abdel-Razzaq, H.-E. Lee, C. Adachi, P. E. Burrows, S. R. Forrest and M. E. Thompson, *J. Am. Chem. Soc.*, 2001, **123**, 4304-4312.

[40] S. M. Borisov and I. Klimant, *Anal. Chem.*, 2007, **79**, 7501-7509.

[41] N. Yanai, K. Suzuki, T. Ogawa, Y. Sasaki, N. Harada and N. Kimizuka, *J. Phys. Chem. A*, 2019, **123**, 10197-10203.

[42] M. Grabolle, M. Spieles, V. Lesnyak, N. Gaponik, A. Eychmüller and U. Resch-Genger, *Anal. Chem.*,

2009, **81**, 6285-6294.

[43] K. Rurack and M. Spieles, *Anal. Chem.*, 2011, **83**, 1232-1242.

[44] Y. Zhou, F. N. Castellano, T. W. Schmidt and K. Hanson, *ACS Energy Lett.*, 2020, **5**, 2322-2326.

[45] J. C. De Mello, H. F. Wittmann and R. H. Friend, *Adv. Mater.*, 1997, **9**, 230-232.

[46] E. Radiunas, S. Raišys, S. Juršėnas, A. Jozeliūnaitė, T. Javorskis, U. Šinkevičiūtė, E. Orentas and K. Kazlauskas, *J. Mater. Chem. C*, 2020, **8**, 5525-5534.

[47] Gaussian 16, Revision B.01, M. J. Frisch, G. W. Trucks, H. B. Schlegel, G. E. Scuseria, M. A. Robb, J. R. Cheeseman, G. Scalmani, V. Barone, G. A. Petersson, H. Nakatsuji, X. Li, M. Caricato, A. V. Marenich, J. Bloino, B. G. Janesko, R. Gomperts, B. Mennucci, H. P. Hratchian, J. V. Ortiz, A. F. Izmaylov, J. L. Sonnenberg, D. Williams-Young, F. Ding, F. Lipparini, F. Egidi, J. Goings, B. Peng, A. Petrone, T. Henderson, D. Ranasinghe, V. G. Zakrzewski, J. Gao, N. Rega, G. Zheng, W. Liang, M. Hada, M. Ehara, K. Toyota, R. Fukuda, J. Hasegawa, M. Ishida, T. Nakajima, Y. Honda, O. Kitao, H. Nakai, T. Vreven, K. Throssell, J. A. Montgomery, Jr., J. E. Peralta, F. Ogliaro, M. J. Bearpark, J. J. Heyd, E. N. Brothers, K. N. Kudin, V. N. Staroverov, T. A. Keith, R. Kobayashi, J. Normand, K. Raghavachari, A. P. Rendell, J. C. Burant, S. S. Iyengar, J. Tomasi, M. Cossi, J. M. Millam, M. Klene, C. Adamo, R. Cammi, J. W. Ochterski, R. L. Martin, K. Morokuma, O. Farkas, J. B. Foresman, and D. J. Fox, Gaussian, Inc., Wallingford CT, 2016.

[48] M. Pope and C. E. Swenberg, *Electronic Processes in Organic Crystals and Polymers*, Oxford University Press, New York, 1999.

[49] A. Monguzzi, J. Mezyk, F. Scotognella, R. Tubino and F. Meinardi, *Phys. Rev. B*, 2008, **78**, 195112.

[50] Y. Y. Cheng, T. Khoury, R. G. C. R. Clady, M. J. Y. Tayebjee, N. J. Ekins-Daukes, M. J. Crossley and T. W. Schmidt, *Phys. Chem. Chem. Phys.*, 2010, **12**, 66-71.

[51] A. Haefele, J. Blumhoff, R. S. Khnayzer and F. N. Castellano, *J. Phys. Chem. Lett.*, 2012, **3**, 299-303.

[52] T. Takata, J. Jiang, Y. Sakata, M. Nakabayashi, N. Shibata, V. Nandal, K. Seki, T. Hisatomi and K. Domen, *Nature*, 2020, **581**, 411-414.

Chapter 3 Efficient Visible-to-UV Photon Upconversion by Porous Film Impregnation Method

3-1 Introduction

Triplet-triplet annihilation-based photon upconversion (TTA-UC) can use low-energy photons to produce higher-energy photons at low excitation intensities.[1-19] TTA-UC typically occurs within triplet donors (sensitizers) and acceptors (emitters) (Figure 3-1). The general TTA-UC starts with the generation of an excited triplet state ($T_{1,D}$) of the donor by light absorption via intersystem crossing (ISC) from an excited singlet state ($S_{1,D}$). The generated triplet energy of the donor is then transferred to the acceptor in a process called triplet energy transfer (TET). During their lifetime, the sensitized acceptor triplets ($T_{1,A}$) annihilate to form an excited singlet state ($S_{1,A}$) of the acceptor. Upconverted emission is obtained from the singlet state with energy higher than the donor absorption. TTA-UC systems have been extensively studied, which convert visible light to UV (λ < 400 nm) light.[20-38] It is applicable to a wide range of photochemical reactions, including solar hydrogen production.[29, 39-41] While the efficiency of TTA-UC for visible-to-UV systems has been limited to below 10% due to the lack of suitable UV-emitting acceptors with a low T_1 energy level, recent research efforts to find better chromophores have yielded significant advances, including the combination of 1,4-bis((triisopropylsilyl)ethynyl)naphthalene (TIPS-Nph) and $Ir(C6)_2(acac)$ described in Chapter 2.[33, 34] B. Albinsson and co-workers have reported the highest efficiency of 26.2% by combining TIPS-Nph with a TADF-type donor 4CzBN in solution.[36] O. S. Wenger and C. Kerzig *et al.* have used a couple of visible-to-UV upconverting chromophores for challenging photoreactions.[29]

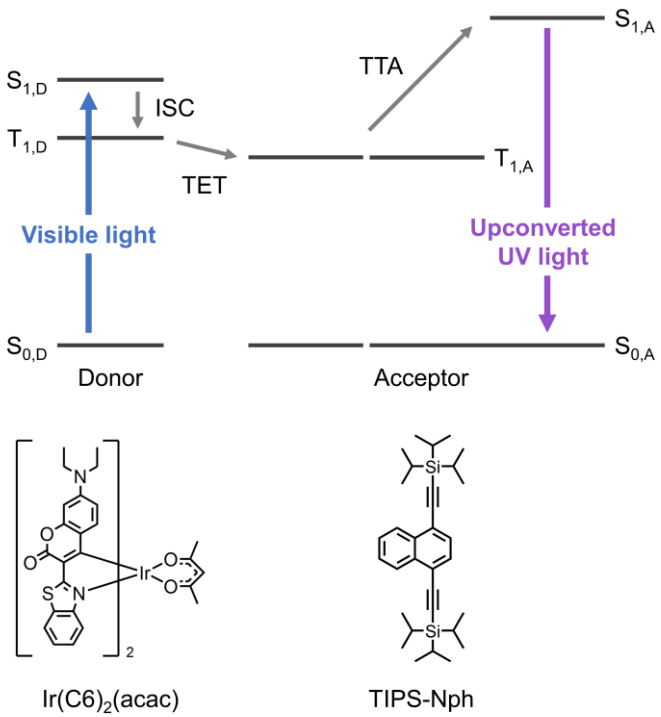

Figure 3-1 Typical TTA-UC mechanism with chemical structures of $Ir(C6)_2(acac)$ as a donor and TIPS-Nph as an acceptor.

For practical applications, achieving TTA-UC in films is particularly desirable.[25, 42-46] However, the examples of films exhibiting visible-to-UV TTA-UC have been limited, and their TTA-UC efficiencies (η_{UC}) are modest, such as 2.6% in a polyurethane film containing Ir(ppy-DBP) and a pyrene derivative (DBP) by Y. Ma *et al.* and 8.6% in neat 2,5-diphenyloxazole (PPO) doped with CBDAC reported by Y. Murakami *et al.*[25, 28, 47, 48] Recent research has discovered new chromophores, and using these dyes is expected to improve the visible-to-UV TTA-UC efficiency of the films.

This chapter reports the highest visible-to-UV TTA-UC efficiency (η_{UC}) of 27.6% as a film sample prepared by a simple porous film impregnation method. This method introduces an upconverting low-volatile solution into a porous film. Thus, TTA-UC occurs in the molecular-diffusion mechanism. Hexyl benzoate was used as the low-volatile solvent, which was reported to have excellent TTA-UC properties by C. Weder and A. Monguzzi *et al.*[49] TIPS-Nph and $Ir(C6)_2(acac)$ were used as the acceptor and the donor, respectively. The resulting film showed the highest η_{UC} of 27.6% by maintaining the excellent performance of the solution and reducing the inner filter effect. Furthermore, combining the film with a microlens array reduced the threshold excitation intensity (I_{th}) to less than 0.60 mW cm^{-2}, much lower than the sunlight intensity (Figure 3-2).

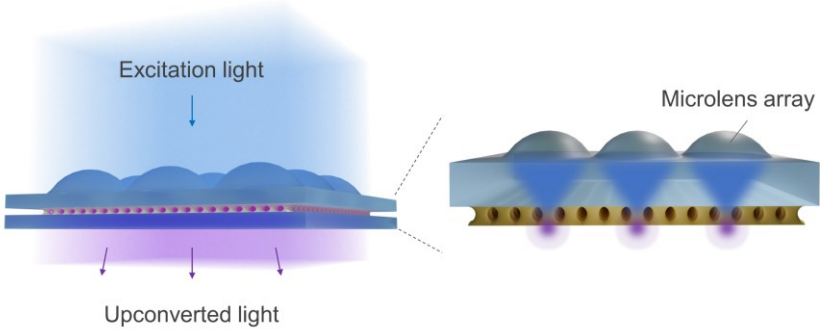

Figure 3-2 Schematic illustration of a porous film integrated with a microlens array.

3-2 Experimental section

3-2-1 Experimental apparatuses

UV-vis absorption spectra were measured using a V-670 and V-770 (JASCO). Photoluminescence (PL) spectra were obtained with an FP-8700 (JASCO). Absolute PL quantum yields were measured using a C10027-01 multichannel analyzer with an integrating sphere (Hamamatsu Photonics). Time-resolved PL lifetime measurements were performed with a TCSPC lifetime spectroscopy system, Quantaurus-Tau C11367-02 and C11567-01 (Hamamatsu Photonics). The viscosity of hexyl benzoate was obtained with a VM-10A-L (SEKONIC CORPORATION) using an NCB2500 (EYELA) as a constant temperature bath. The validity of the viscosity was confirmed by comparing the experimental value of 1-hexanol (4.28 cP at 25 °C) with the reported values (4.436[50], 4.594[51], 4.403[52]). Scanning electron microscopy (SEM) images were obtained using a Zeiss Ultra55 instrument at the Ultramicroscopy Center, Kyushu University. Thermogravimetric analysis (TGA) was performed under a flow of N_2 gas (approximately 100 mL min^{-1}) using a Thermo plus EV02 TG8120 (Rigaku). The thickness of the porous films was measured with a micrometer MCD130-25 (Niigata Seiki).

For TTA-UC measurements, a diode laser with a wavelength of 445 nm (75 mW, RGB Photonics) was used as the excitation light source. Laser intensity and beam profile were measured using a PD300-UV photodiode sensor (OPHIR Photonics) and a CCD beam profiler SP620 (OPHIR Photonics). The diameter of the laser beam ($1/e^2$) was determined to be 3.9×10^{-4} and 1.2×10^{-3} cm^2 with and without a focus lens at the sample position, respectively. The laser power was controlled by rotating variable neutral density (ND) filters. An MCPD-9800 (Otsuka Electronics) was used to obtain PL spectra, and a standard lamp HL-3 plus-CAL (Ocean Optics) was used to calibrate the spectra ($\lambda >$ 350 nm), including achromatic lenses in front of the detector. In the measurement, the detector captures the emission from the same surface where the laser hits (Figure 3-3).

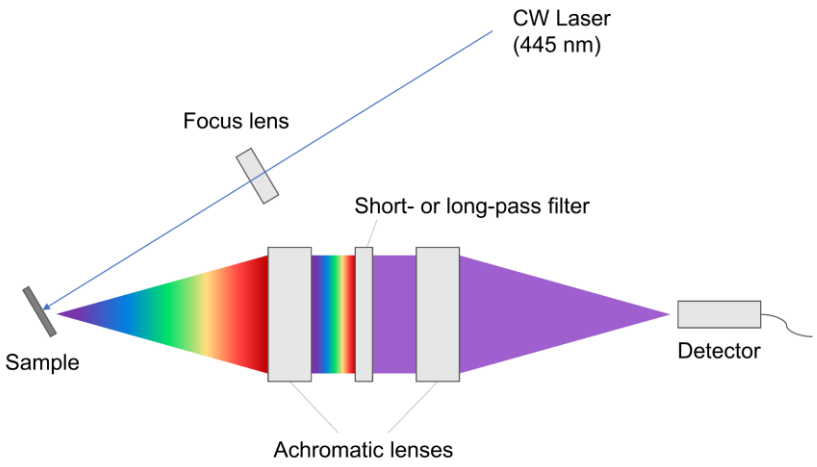

Figure 3-3 Illustration of the measurement setup for TTA-UC.

3-2-2 Calculation of TTA-UC efficiency

The TTA-UC efficiency (η_{UC}) in solution was calculated by a relative method using the following equation,[2, 53]

$$\eta_{UC} = 2\Phi_{std}\left(\frac{1-10^{-A}_{std}}{1-10^{-A}_{UC}}\right)\left(\frac{E_{UC}}{E_{std}}\right)\left(\frac{I_{std}}{I_{UC}}\right)\left(\frac{n_{UC}}{n_{std}}\right)^2 \quad \text{(Eq. 3-1)}$$

where Φ, A, E, I, and n are the quantum yield, absorbance at a laser wavelength, integrated photoluminescence spectral profile, excitation intensity, and refractive index of the solvent, respectively. The subscripts UC and std denote the upconversion and standard systems, respectively.

The efficiency of TTA-UC in the form of films was determined by the relative method using donor phosphorescence (phos) as the internal standard, according to the following equation,

$$\eta_{UC} = 2\Phi_{phos}\left(\frac{E_{UC}}{E_{phos}}\right)\left(\frac{I_{phos}}{I_{UC}}\right) \quad \text{(Eq. 3-2)}$$

A value of Φ_{phos} was measured by the absolute PL quantum yield measurement using the integrating sphere and was found to be 8.6% in the spectral region from 500 to 800 nm excited by 445 nm.

3-2-3 Estimation of triplet lifetime

To evaluate the TTA-UC properties in detail, the acceptor triplet lifetime was estimated by the following equation,[54]

$$I_{UC}(t) \propto \exp\left(\frac{-t}{\tau_{UC}}\right) = \exp\left(\frac{-2t}{\tau_T}\right) \quad \text{(Eq. 3-3)}$$

where τ_{UC} and τ_T are the lifetime of the UC and the lifetime of the acceptor triplet, respectively.

3-2-4 Materials

All reagents and solvents were used as received without further purification unless noted. The synthesis and characterization of TIPS-Nph are described in the literature.[33, 36] $Ir(C6)_2(acac)$ was purchased from NARD Institute, Ltd. and recrystallized using ethanol and chloroform. For photophysical and TTA-UC measurements, all samples were prepared in an argon-filled glovebox ($[O_2] < 0.1$ ppm). Hexyl benzoate was purchased from TCI and deaerated by vacuuming with an oil-sealed rotary pump (TSW-150, SATO VAC INC.). As a porous film, Microporous Film (CMZ-05076, catalog thickness 38 μm) was purchased from 3M and used as received. A microlens array was provided by Ushio Inc. A focal diameter of the microlens array was estimated to be approximately 3.0 μm by geometric optical calculation using a single wavelength of 445 nm.

3-3 Results and discussion

3-3-1 Photophysical and TTA-UC properties in solution

Before evaluating TTA-UC in film form, typical photophysical and TTA-UC properties in bulk solution were investigated. A deaerated hexyl benzoate solution of TIPS-Nph was prepared in an argon-filled glovebox ([TIPS-Nph] = 100 μM, 10 mM). Hexyl benzoate is a low-volatile solvent with a boiling point above 200 ℃[55] and transmittance in the wavelength region above 350 nm as high as that of THF (Figure 3-4). The absorption spectrum of the diluted solution showed a maximum absorption peak at 352 nm (Figure 3-5), which is almost the same as that in THF (350 nm). In the photoluminescence spectra, vibronic emission peaks of 361 and 374 nm were observed in the 100 μM solution. On the other hand, the 10 mM solution showed a peak at 376 nm due to the self-absorption at the shorter wavelengths. The fluorescence quantum yields of the 100 μM and 10 mM solutions were 76.3% and 71.0%, respectively (λ_{ex} = 320 nm). These values are similar to the reported ones (74% and 66%) in THF,[33] indicating that photophysical states in hexyl benzoate are inherently unchanged.

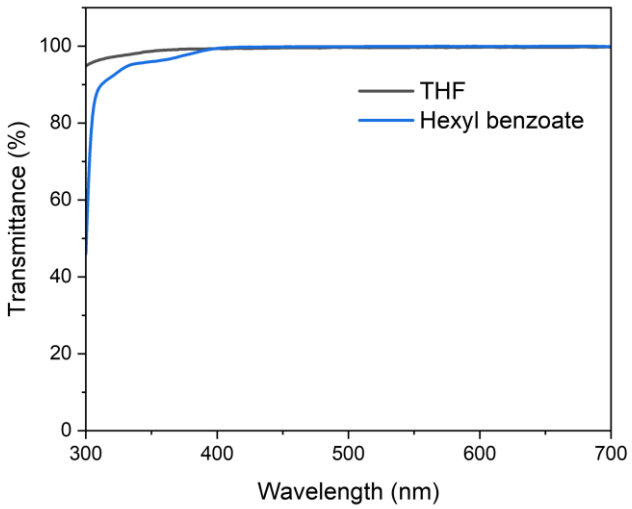

Figure 3-4 Transmittance of THF and hexyl benzoate in a quartz cell with a 5 mm effective optical path length.

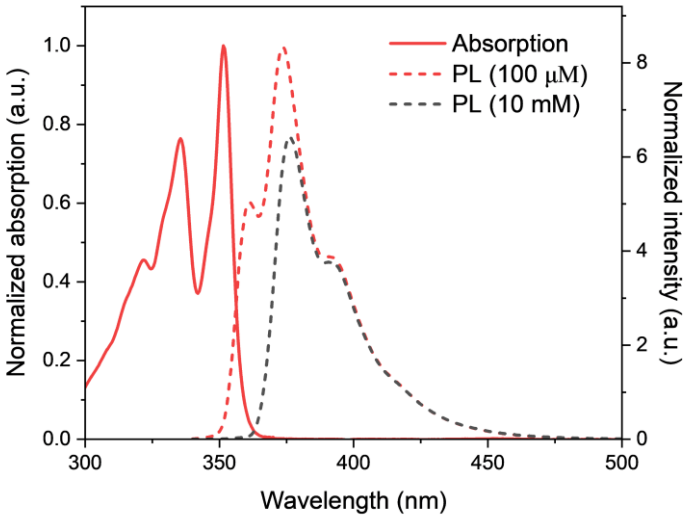

Figure 3-5 Normalized absorption (solid, red) and PL (dashed, red, λ_{ex} = 320 nm) spectra of TIPS-Nph in deaerated hexyl benzoate (100 μM), and normalized PL spectrum of TIPS-Nph (10 mM) (dashed, gray, λ_{ex} = 320 nm). PL spectra were normalized at 420 nm.

To evaluate the TTA-UC properties, a deaerated hexyl benzoate solution of TIPS-Nph and Ir(C6)$_2$(acac) was prepared in the glovebox ([TIPS-Nph] = 10 mM, [Ir(C6)$_2$(acac)] = 100 μM). Upon irradiation with a 445 nm laser, the solution showed upconverted emission in the UV region below 400 nm (Figure 3-6). The TTA-UC efficiency (η_{UC}) was found to be 16.7% at 7.0 W cm^{-2} by the relative method using coumarin 6 as the standard, which is close to the previously reported value of 20.5% in a THF solution of the same TIPS-Nph and Ir(C6)$_2$(acac) combination.[33]

The efficiency of TTA-UC can be expressed by the following equation,[7]

$$\eta_{UC} = f\Phi_{ISC}\Phi_{TET}\Phi_{TTA}\Phi_{FL} \quad \text{(Eq. 3-4)}$$

where f is the spin statistical factor (singlet generation efficiency), Φ_{ISC}, Φ_{TET}, Φ_{TTA}, and Φ_{FL} are the efficiencies of ISC, TET, TTA, and acceptor fluorescence, respectively. Φ_{ISC} and Φ_{TTA} can be approximated by 100% in the current system because the donor fluorescence was not observed, and the TTA-UC efficiency was estimated at the high excitation intensity above I_{th}, which will be discussed later. The value of Φ_{TET} was determined to be 90.6% using the following equation,

$$\Phi_{TET} = 1 - \frac{\Phi_P}{\Phi_{P,0}} \quad \text{(Eq. 3-5)}$$

where Φ_P and $\Phi_{P,0}$ are the phosphorescence quantum yields of the donor with and without the acceptor, respectively. The acceptor showed a Φ_{FL} of 71.0% at a concentration of 10 mM in hexyl benzoate. Using Eq. 3-4 with these parameters, an f value of 26.0% was estimated, which is close to that in THF (32%).[33] Note that this is a conservative estimate of the f value due to the inner filter effect and

acceptor-to-donor back energy transfer.[36]

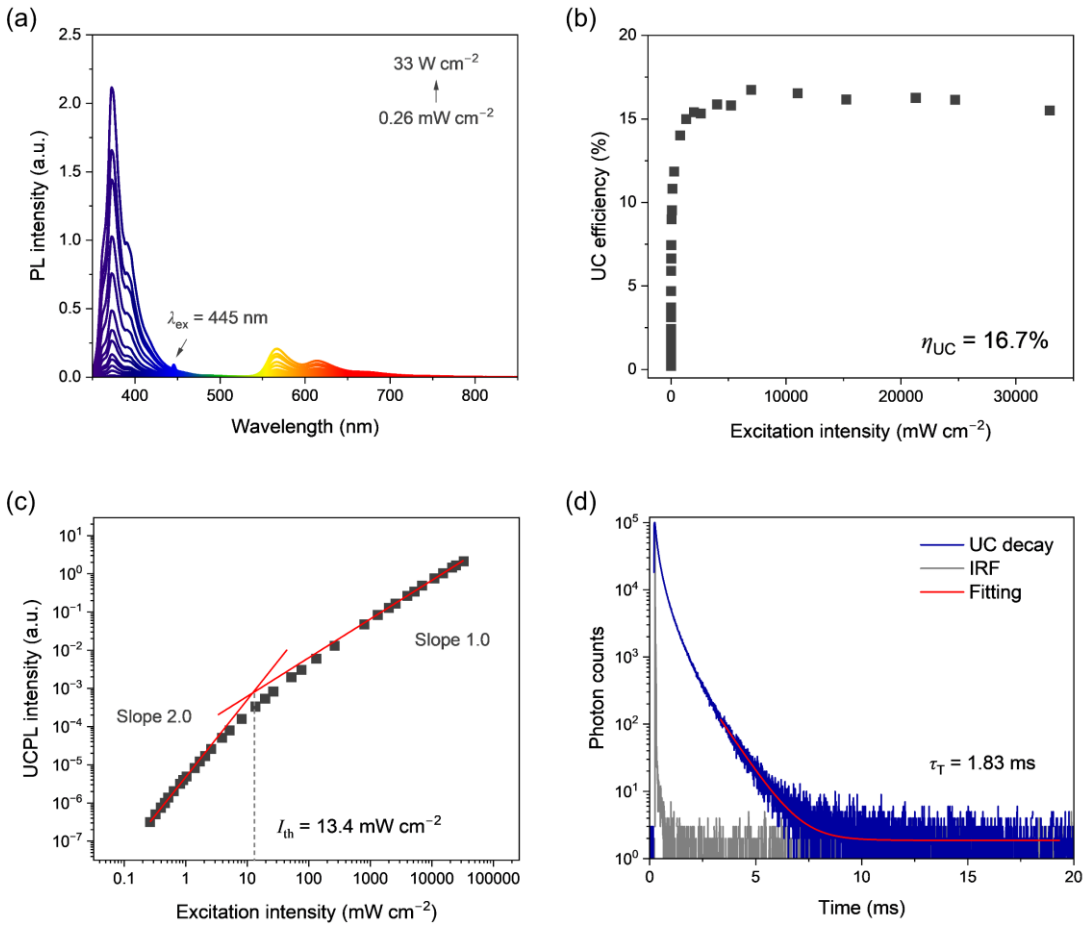

Figure 3-6 (a) PL spectra, (b) TTA-UC efficiencies, and (c) UCPL intensities of a deaerated hexyl benzoate solution of TIPS-Nph (10 mM) and Ir(C6)$_2$(acac) (100 μM) with different excitation intensities under a laser (λ_{ex} = 445 nm). (d) Upconversion emission decay (blue) of the hexyl benzoate solution at 380 nm under pulsed excitation light with a band-pass filter of 445 nm. The gray line shows the instrumental response function (IRF).

The threshold excitation intensity (I_{th}), a fundamental parameter of TTA-UC to optimize the TTA process, was then evaluated. As a result, the I_{th} value in hexyl benzoate was found to be 13.4 mW cm^{-2}, about 5.8 times higher than the reported value in THF (2.3 mW cm^{-2}).[33] The I_{th} in solution systems can be expressed by the following equation,[56-58]

$$I_{th} = \frac{1}{8\pi a_0 \Phi_{ISC} \Phi_{TET} D_T \tau_T^2} \quad \text{(Eq. 3-6)}$$

where a_0 is the effective distance of TTA, α is a donor absorption coefficient, D_T is a triplet diffusion

constant, and τ_T is an acceptor triplet lifetime. The donor absorption in hexyl benzoate showed no significant difference from that in THF (Figure 3-7). The triplet diffusion constant can be considered as the molecular diffusion coefficient in solution and can be approximated by the Stokes-Einstein equation,[59]

$$D_T = \frac{k_B T}{6\pi\mu R} \qquad \text{(Eq. 3-7)}$$

where k_B is the Boltzmann constant, T is temperature, μ is a solvent viscosity, and R is the molecular radius. As seen from the above equation (Eq. 3-6 and 3-7), TTA-UC depends on the viscosity of the solvent.[60, 61] The viscosity of hexyl benzoate was measured to be 4.54 cP at 25 °C, and that of THF was reported to be 0.46 cP at 25 °C.[62, 63] The triplet lifetime of the acceptor was 1.83 and 0.88 ms in hexyl benzoate and THF, respectively.[33] Using these experimental parameters and assuming that the effective distance (a_0) on TTA is independent of the solvent, I_{th} is predicted to be 1.9 times higher in hexyl benzoate than in THF. This prediction differs slightly from the observed 5.8-fold difference. While the exact reason for this difference is not apparent at the present moment, the effective triplet-triplet interaction might be different in different solvents.

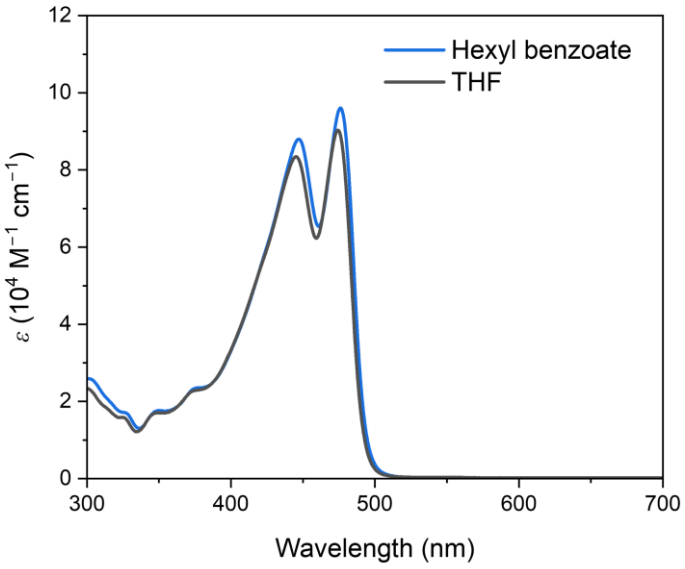

Figure 3-7 Absorption spectra of $Ir(C6)_2(acac)$ in hexyl benzoate and THF (100 μM).

3-3-2 Analysis of porous films

For a thin and porous film that is highly transparent in the UV and visible region, a 38 μm thick polypropylene-based porous film (Microporous Film, 3M) was selected. This porous film was found to have a sponge structure from SEM images (Figure 3-8). The refractive index of polypropylene is 1.49,[64] similar to that of hexyl benzoate (1.49),[55] indicating that the immersed porous film has good

transparency. Due to the difference in refractive index between polypropylene and air (1.00),[65] the porous film was initially opaque. However, it became transparent immediately by being immersed in hexyl benzoate (Figure 3-9a). The film thickness did not change with immersion in hexyl benzoate, and no significant swelling behavior was observed (Table 3-1). Thermogravimetric analysis (TGA) of the immersed porous film showed that 43 wt% of hexyl benzoate was incorporated into the film (Figure 3-9b).

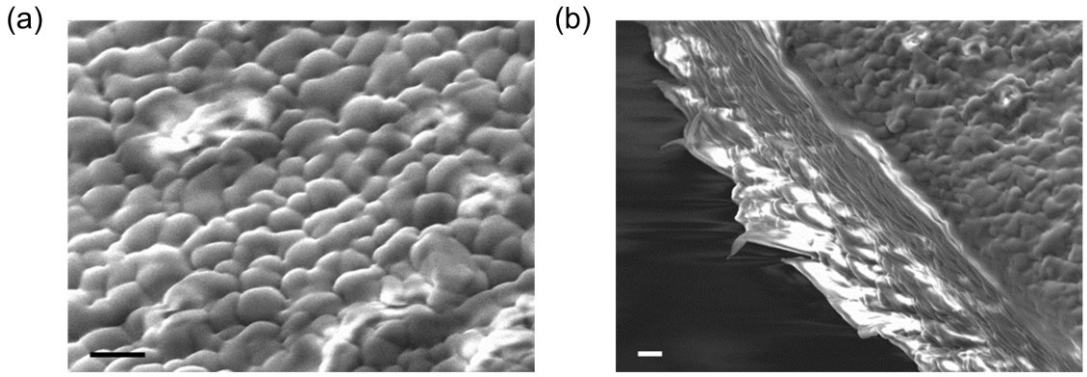

Figure 3-8 SEM images of (a) the surface and (b) the cross-section of a porous film. Scale bars indicate 2 μm.

Table 3-1 Mean and standard deviation (SD) values of porous films. The minimum scale value is 0.001 mm (1 μm).

	Mean (μm)	SD (μm)
Pristine film	40.2	2.04
Immersed film	40.8	1.86

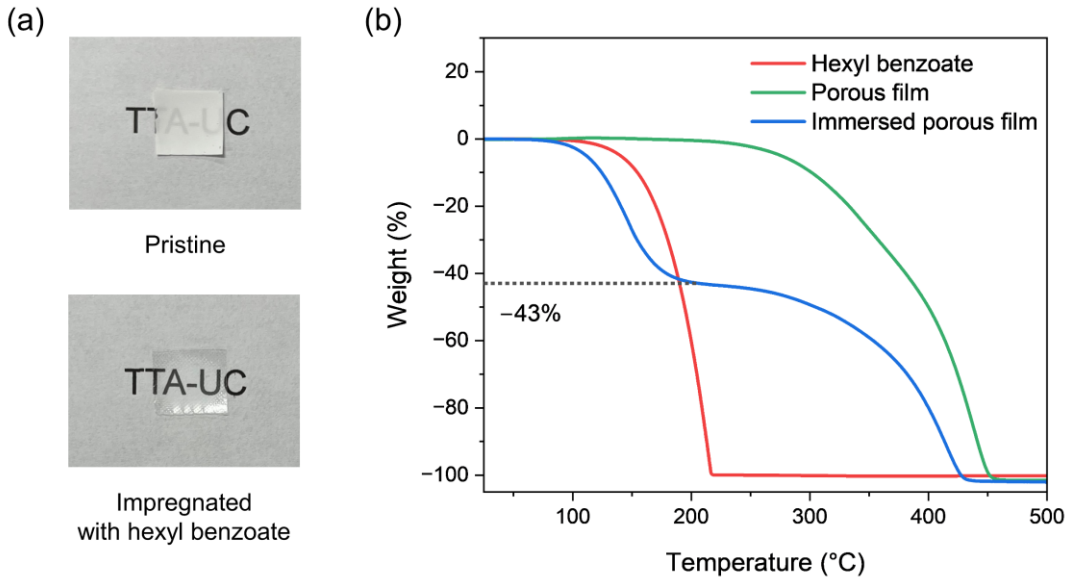

Figure 3-9 (a) Photographs of a pristine porous film and a porous film impregnated with hexyl benzoate. (b) TGA curves of an immersed porous film in hexyl benzoate (blue), hexyl benzoate (red), and pristine porous film (green).

3-3-3 Preparation of TTA-UC films by the porous film impregnation method

To fabricate films that contain UC chromophores, a porous film was impregnated with a hexyl benzoate solution of TIPS-Nph and $Ir(C6)_2(acac)$ in the glovebox ([TIPS-Nph] = 10 mM, $[Ir(C6)_2(acac)]$ = 100 μM). The excess solution was then removed from the surface of the film. The porous film was sandwiched between two quartz substrates, sealed with epoxy resin glue, and left overnight inside the glovebox (Figure 3-10).

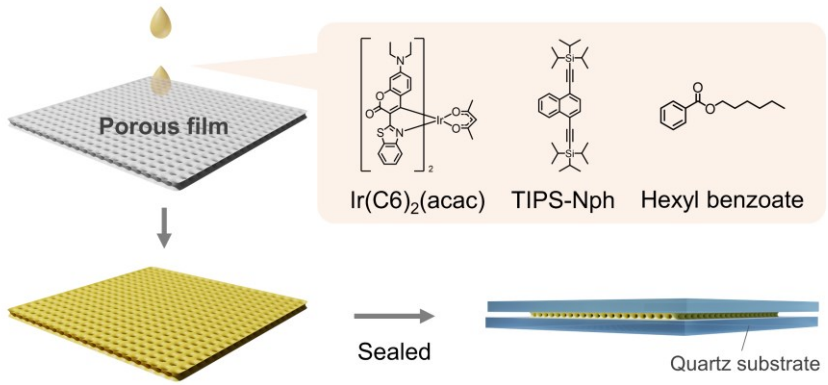

Figure 3-10 Schematic illustration of porous film impregnation method using $Ir(C6)_2(acac)$, TIPS-Nph, and hexyl benzoate as a donor, acceptor, and solvent, respectively.

3-3-4 TTA-UC properties in film form

To characterize TTA-UC properties, the film immersed in hexyl benzoate solution containing TIPS-Nph and $Ir(C6)_2(acac)$ was irradiated with a 445 nm laser, resulting in upconverted emission in the UV range (Figure 3-11a). Note that the film showed an emission peak at 357 nm on the short-wavelength side, which was not observed in the bulk solution (Figure 3-6a). The appearance of this peak should be due to a decrease in the self-absorption of the acceptor emission by shortening the optical path length from 1 mm in the solution to 38 μm in the film.

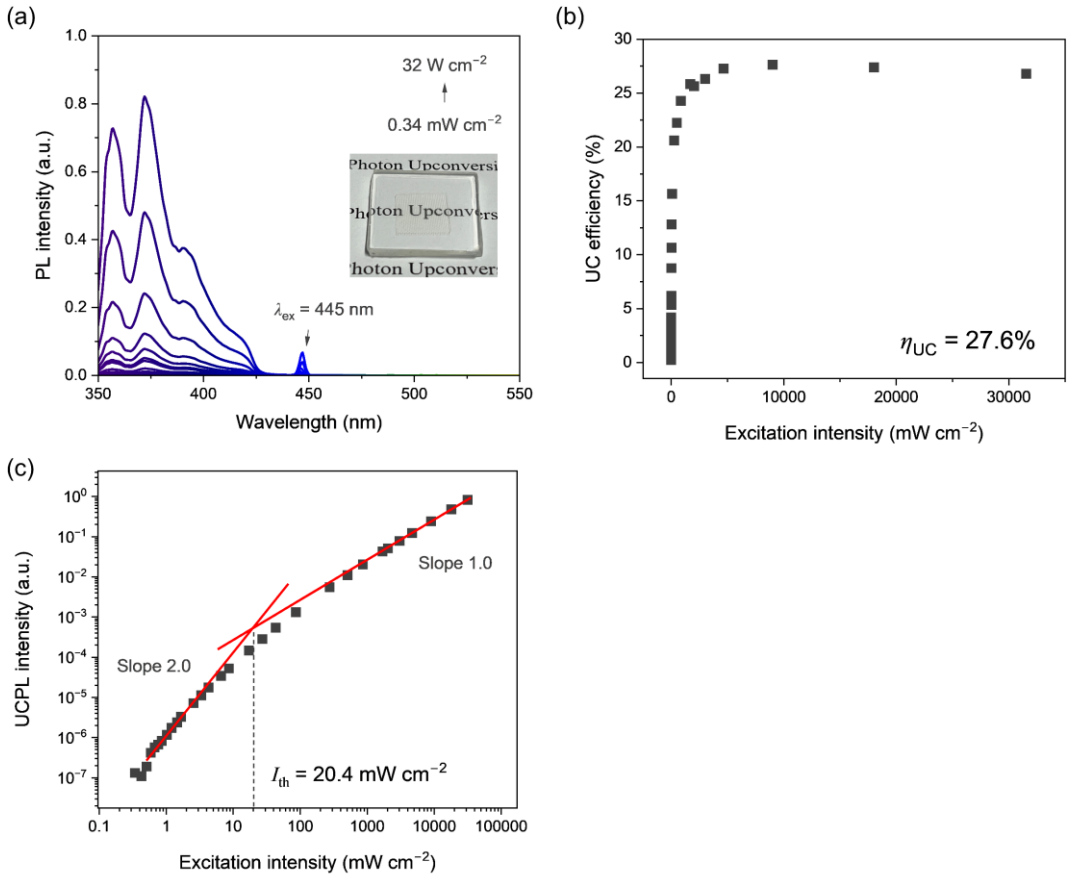

Figure 3-11 (a) PL spectra of the film at various excitation intensities with a short-pass filter (425 nm). Inset is a photograph of the film sealed between quartz substrates. (b) Upconversion efficiencies and (c) UCPL intensities at 372 nm of the film in different excitation intensities.

The TTA-UC efficiency of this film was then measured by the relative method using the phosphorescence of $Ir(C6)_2(acac)$ as an internal standard since the slight scattering nature of the film made it difficult to estimate the absorbance precisely. As a result, the film showed the highest visible-to-UV η_{UC} of 27.6% and a relatively low I_{th} of 20.4 mW cm^{-2} (Figure 3-11b, c). The higher efficiency of TTA-UC in the film than in the bulk solution is reasonable, considering the less re-absorption in the thinner sample geometry. This efficiency shows good agreement with the reported calculated value of 33.6% obtained by correcting for re-absorption based on the measured efficiency of 26.2%.[36] Moreover, the upconverted emission intensity was not changed under continuous laser irradiation for 60 min at 1.5 mW cm^{-2}, equivalent to 1sun (1.4 mW cm^{-2} for 445 ± 5 nm[66]) (Figure 3-12a). To evaluate the storage stability of the film, TTA-UC measurements were performed after the film was left in the dark for 9 days. The I_{th} value of the film remained low at 29.1 mW cm^{-2} after storage (Figure 3-12b). In future studies, it will be necessary to systematically investigate how the TTA-UC efficiency varies with pore size, film material, and film thickness to optimize TTA-UC in the thin film.

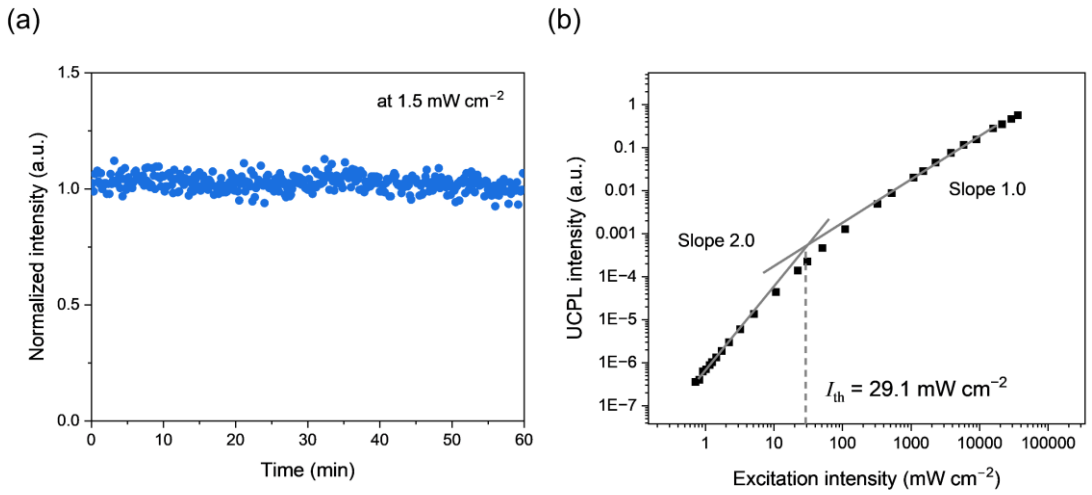

Figure 3-12 (a) UCPL intensities (λ_{det} = 372 nm) normalized at 0 min of an upconverting film sealed with quartz substrates at 1.5 mW cm^{-2} for one hour. (b) UCPL intensities of a film stored in the dark for 9 days at different excitation intensities under a 445 nm laser.

3-3-5 Combination of the microlens array

Polymer lens arrays and microcavities were used to reduce the excitation intensity and to achieve efficient upconversion.[67-70] In this study, taking advantage of the fact that the film prepared by the porous film impregnation method can be combined with any substrate, a microlens array was selected to reduce the threshold excitation intensity (I_{th}). Microlens arrays can focus the excitation light onto the film. The microlens array is made of quartz and has a diameter of 124 μm and a pitch of 128 μm with a calculated focus diameter of approximately 3.0 μm (1708×) and a focus distance of 15−30 μm from the bottom of the microlens array (Figure 3-13). The porous film containing the hexyl benzoate solution was placed just below the microlens array. The thickness of the upconverting porous film is 38 μm (see 3-3-2), allowing the light to be focused inside the film.

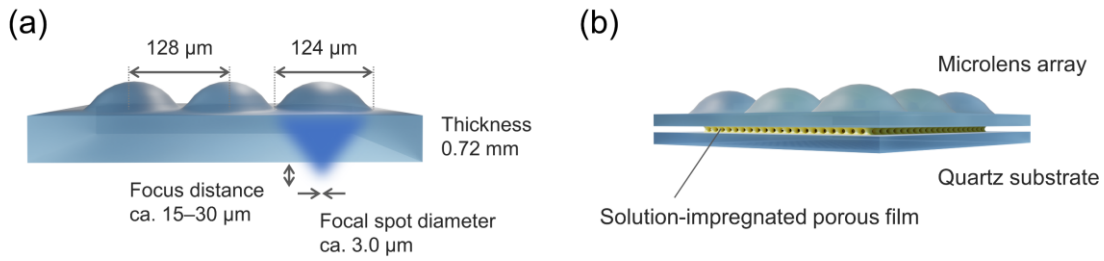

Figure 3-13 Schematic illustration of (a) a microlens array and (b) a sandwiched sample structure.

3-3-6 TTA-UC properties in the film with the microlens array

In a measurement using a microlens array, the porous film was sandwiched between a quartz

substrate on one side and the microlens array on the other, sealed with the epoxy resin glue, and left in the glovebox overnight.

Under the laser irradiation at a wavelength of 445 nm, the combined film with the microlens array showed an I_{th} value of less than 0.60 mW cm^{-2}, corresponding to 0.43 sun (Figure 3-14). Because the I_{th} was too low, only up to a slope of 1.3 could be observed in this measurement, not up to a slope of 2. Therefore, the actual I_{th} was too low to be determined and should be lower than 0.60 mW cm^{-2}. It is to be noted that the linear region was observed from 8.7 mW cm^{-2}, suggesting that TTA occurs efficiently around the solar light intensity. Solutions exhibiting TTA-UC from visible to UV light have been widely studied. However, it is not easy to combine them with microlens arrays. Although conventional films can be easily combined with microlens arrays, obtaining efficient visible-to-UV TTA-UC in film form has been difficult. The newly developed porous film impregnation method can easily prepare a film while maintaining the high TTA-UC efficiency of the solution. It can utilize subsolar intensity light when combined with a microlens array.

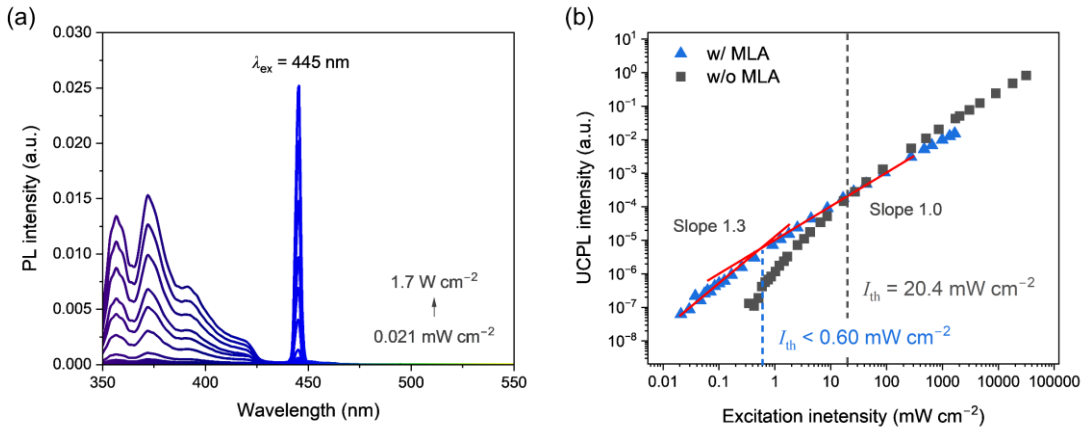

Figure 3-14 (a) PL spectra of the film integrated with the microlens array at various excitation intensities with a 425 nm short-pass filter. (b) PL intensities at 372 nm of the film integrated with (blue triangle) and without (gray square, the same data in Figure 3-11c) a microlens array (MLA) at different excitation intensities.

3-4 Conclusion

In conclusion, this work has developed the film with the highest visible-to-UV TTA-UC efficiency of 27.6% to date and found a way to utilize subsolar light by combining the film with the microlens array. The method of impregnating the porous film with the low-volatile upconverting solution is straightforward and powerful, making it possible to fabricate the film while maintaining the high TTA-UC performance of the bulk solution. In addition, the film can be combined with the microlens array to harvest subsolar-intensity light. This film would enable the generation of UV light under weak visible light, including sunlight and indoor LED light, for various applications such as artificial photosynthesis, environmental purification, and water purification. Furthermore, the newly developed method is highly versatile and can be applied to other excitation wavelengths, such as green, red, and near-IR light, by simply changing the type of dye.

3-5 References

[1] S. Baluschev, T. Miteva, V. Yakutkin, G. Nelles, A. Yasuda and G. Wegner, *Phys. Rev. Lett.*, 2006, **97**, 143903.

[2] T. N. Singh-Rachford and F. N. Castellano, *Coord. Chem. Rev.*, 2010, **254**, 2560-2573.

[3] J. Zhao, S. Ji and H. Guo, *RSC Adv.*, 2011, **1**, 937-950.

[4] J.-H. Kim and J.-H. Kim, *J. Am. Chem. Soc.*, 2012, **134**, 17478-17481.

[5] R. Andernach, H. Utzat, S. D. Dimitrov, I. McCulloch, M. Heeney, J. R. Durrant and H. Bronstein, *J. Am. Chem. Soc.*, 2015, **137**, 10383-10390.

[6] V. Gray, D. Dzebo, M. Abrahamsson, B. Albinsson and K. Moth-Poulsen, *Phys. Chem. Chem. Phys.*, 2014, **16**, 10345-10352.

[7] A. Monguzzi, R. Tubino, S. Hoseinkhani, M. Campione and F. Meinardi, *Phys Chem Chem Phys*, 2012, **14**, 4322-4332.

[8] Y. C. Simon and C. Weder, *J. Mater. Chem.*, 2012, **22**, 20817-20830.

[9] M. Wu, D. N. Congreve, M. W. B. Wilson, J. Jean, N. Geva, M. Welborn, T. Van Voorhis, V. Bulović, M. G. Bawendi and M. A. Baldo, *Nat. Photon.*, 2016, **10**, 31-34.

[10] N. Yanai and N. Kimizuka, *Acc. Chem. Res.*, 2017, **50**, 2487-2495.

[11] E. M. Gholizadeh, S. K. K. Prasad, Z. L. Teh, T. Ishwara, S. Norman, A. J. Petty II, J. H. Cole, S. Cheong, R. D. Tilley, J. E. Anthony, S. Huang and T. W. Schmidt, *Nat. Photon.*, 2020, **14**, 585-590.

[12] S. P. Hill and K. Hanson, *J. Am. Chem. Soc.*, 2017, **139**, 10988-10991.

[13] Z. Huang and M. L. Tang, *J. Am. Chem. Soc.*, 2017, **139**, 9412-9418.

[14] C. J. Imperiale, P. B. Green, E. G. Miller, N. H. Damrauer and M. W. B. Wilson, *J. Phys. Chem. Lett.*, 2019, **10**, 7463-7469.

[15] B. D. Ravetz, A. B. Pun, E. M. Churchill, D. N. Congreve, T. Rovis and L. M. Campos, *Nature*, 2019, **565**, 343-346.

[16] J. M. Rowe, J. Zhu, E. M. Soderstrom, W. Xu, A. Yakovenko and A. J. Morris, *Chem. Commun.*, 2018, **54**, 7798-7801.

[17] R. Sato, H. Kitoh-Nishioka, K. Kamada, T. Mizokuro, K. Kobayashi and Y. Shigeta, *J. Phys. Chem. Lett.*, 2018, **9**, 6638-6643.

[18] S. Wieghold, A. S. Bieber, Z. A. VanOrman, L. Daley, M. Leger, J.-P. Correa-Baena and L. Nienhaus, *Matter*, 2019, **1**, 705-719.

[19] X. Yang, J. Han, Y. Wang and P. Duan, *Chem. Sci.*, 2019, **10**, 172-178.

[20] Q. Chen, Y. Liu, X. Guo, J. Peng, S. Garakyaraghi, C. M. Papa, F. N. Castellano, D. Zhao and Y. Ma, *J. Phys. Chem. A*, 2018, **122**, 6673-6682.

[21] P. Duan, N. Yanai and N. Kimizuka, *Chem. Commun.*, 2014, **50**, 13111-13113.

[22] V. Gray, P. Xia, Z. Huang, E. Moses, A. Fast, D. A. Fishman, V. I. Vullev, M. Abrahamsson, K. Moth-Poulsen and M. L. Tang, *Chem. Sci.*, 2017, **8**, 5488-5496.

[23] S. He, X. Luo, X. Liu, Y. Li and K. Wu, *J. Phys. Chem. Lett.*, 2019, **10**, 5036-5040.

[24] S. Hisamitsu, J. Miyano, K. Okumura, J. K.-H. Hui, N. Yanai and N. Kimizuka, *ChemistryOpen*, 2020, **9**, 14-17.

[25] X. Jiang, X. Guo, J. Peng, D. Zhao and Y. Ma, *ACS Appl. Mater. Interfaces*, 2016, **8**, 11441-11449.

[26] Y. Kawashima, H. Kouno, K. Orihashi, K. Nishimura, N. Yanai and N. Kimizuka, *Mol. Syst. Des. Eng.*, 2020, **5**, 792-796.

[27] K. Okumura, N. Yanai and N. Kimizuka, *Chem. Lett.*, 2019, **48**, 1347-1350.

[28] J. Peng, X. Guo, X. Jiang, D. Zhao and Y. Ma, *Chem. Sci.*, 2016, **7**, 1233-1237.

[29] B. Pfund, D. M. Steffen, M. R. Schreier, M. S. Bertrams, C. Ye, K. Börjesson, O. S. Wenger and C. Kerzig, *J. Am. Chem. Soc.*, 2020, **142**, 10468-10476.

[30] T. N. Singh-Rachford and F. N. Castellano, *J. Phys. Chem. A*, 2009, **113**, 5912-5917.

[31] N. Yanai, M. Kozue, S. Amemori, R. Kabe, C. Adachi and N. Kimizuka, *J. Mater. Chem. C*, 2016, **4**, 6447-6451.

[32] W. Zhao and F. N. Castellano, *J. Phys. Chem. A*, 2006, **110**, 11440-11445.

[33] N. Harada, Y. Sasaki, M. Hosoyamada, N. Kimizuka and N. Yanai, *Angew. Chem. Int. Ed.*, 2021, **60**, 142-147.

[34] M. Uji, N. Harada, N. Kimizuka, M. Saigo, K. Miyata, K. Onda and N. Yanai, *J. Mater. Chem. C*, 2022, **10**, 4558-4562.

[35] Y. Murakami, A. Motooka, R. Enomoto, K. Niimi, A. Kaiho and N. Kiyoyanagi, *Phys Chem Chem Phys*, 2020, **22**, 27134-27143.

[36] A. Olesund, J. Johnsson, F. Edhborg, S. Ghasemi, K. Moth-Poulsen and B. Albinsson, *J. Am. Chem. Soc.*, 2022, **144**, 3706-3716.

[37] T. J. B. Zähringer, M.-S. Bertrams and C. Kerzig, *J. Mater. Chem. C*, 2022, **10**, 4568-4573.

[38] B. Yurash, A. Dixon, C. Espinoza, A. Mikhailovsky, S. Chae, H. Nakanotani, C. Adachi and T.-Q. Nguyen, *Adv. Mater.*, 2022, **34**, 2103976.

[39] M. Barawi, F. Fresno, R. Pérez-Ruiz and V. A. de la Peña O'Shea, *ACS Appl. Energy Mater.*, 2019, **2**, 207-211.

[40] F. Glaser, C. Kerzig and O. S. Wenger, *Chem. Sci.*, 2021, **12**, 9922-9933.

[41] T. J. B. Zähringer, J. A. Moghtader, M.-S. Bertrams, B. Roy, M. Uji, N. Yanai and C. Kerzig, *Angew. Chem. Int. Ed.*, 2023, **62**, e202215340.

[42] A. J. Svagan, D. Busko, Y. Avlasevich, G. Glasser, S. Baluschev and K. Landfester, *ACS Nano*, 2014, **8**, 8198-8207.

[43] M. Kinoshita, Y. Sasaki, S. Amemori, N. Harada, Z. Hu, Z. Liu, L. K. Ono, Y. Qi, N. Yanai and N. Kimizuka, *ChemPhotoChem*, 2020, **4**, 5271-5278.

[44] R. Vadrucci, A. Monguzzi, F. Saenz, B. D. Wilts, Y. C. Simon and C. Weder, *Adv. Mater.*, 2017, **29**, 1702992.

[45] P. Bharmoria, S. Hisamitsu, Y. Sasaki, T. S. Kang, M.-A. Morikawa, B. Joarder, K. Moth-Poulsen, H. Bildirir, A. Mårtensson, N. Yanai and N. Kimizuka, *J. Mater. Chem. C*, 2021, **9**, 11655-11661.

[46] T. Kashino, R. Haruki, M. Uji, N. Harada, M. Hosoyamada, N. Yanai and N. Kimizuka, *ACS Appl. Mater. Interfaces*, 2022, **14**, 22771-22780.

[47] P. B. Merkel and J. P. Dinnocenzo, *J. Lumin.*, 2009, **129**, 303-306.

[48] R. Enomoto and Y. Murakami, *J. Mater. Chem. C*, 2023, **11**, 1678-1683.

[49] F. Saenz, A. Ronchi, M. Mauri, D. Kiebala, A. Monguzzi and C. Weder, *ACS Appl. Mater. Interfaces*, 2021, **13**, 43314-43322.

[50] G. P. Dubey and R. Kumar, *J. Chem. Thermodyn.*, 2014, **71**, 27-36.

[51] A. S. Al-Jimaz, J. A. Al-Kandary and A.-H. M. Abdul-Latif, *J. Chem. Eng. Data*, 2007, **52**, 206-214.

[52] A. S. Al-Jimaz, J. A. Al-Kandary and A.-H. M. Abdul-Latif, *Fluid Ph. Equilibria*, 2004, **218**, 247-260.

[53] N. Yanai, K. Suzuki, T. Ogawa, Y. Sasaki, N. Harada and N. Kimizuka, *J. Phys. Chem. A*, 2019, **123**, 10197-10203.

[54] M. Pope and C. E. Swenberg, *Electronic Processes in Organic Crystals and Polymers*, Oxford University Press, New York, 1999.

[55] R. L. Merker and M. J. Scott, *J. Org. Chem.*, 1961, **26**, 5180-5182.

[56] A. Monguzzi, J. Mezyk, F. Scotognella, R. Tubino and F. Meinardi, *Phys. Rev. B*, 2008, **78**, 195112.

[57] Y. Y. Cheng, T. Khoury, R. G. C. R. Clady, M. J. Y. Tayebjee, N. J. Ekins-Daukes, M. J. Crossley and T. W. Schmidt, *Phys. Chem. Chem. Phys.*, 2010, **12**, 66-71.

[58] A. Haefele, J. Blumhoff, R. S. Khnayzer and F. N. Castellano, *J. Phys. Chem. Lett.*, 2012, **3**, 299-303.

[59] P. W. Atkins and J. De Paula, *Atkins' Physical Chemistry*, Oxford University Press, Oxford, 10th edn., 2014.

[60] V. R. Nicholas J. Turro, J. C. Scaiano, *Modern Molecular Photochemistry of Organic Molecules*, University Science Books, Sausalito, California, 2010.

[61] Y. Murakami and K. Kamada, *Phys. Chem. Chem. Phys.*, 2021, **23**, 18268-18282.

[62] S. Rodríguez, C. Lafuente, P. Cea, F. M. Royo and J. S. Urieta, *J. Chem. Eng. Data*, 1997, **42**, 1285-1289.

[63] C. Carvajal, K. J. Tölle, J. Smid and M. Szwarc, *J. Am. Chem. Soc.*, 1965, **87**, 5548-5553.

[64] D. W. van Krevelen, *Properties of Polymers : Their Correlation With Chemical Structure; Their Numerical Estimation and Prediction from Additive Group Contributions*, Elsevier, Amsterdam, London, New York, Tokyo, 3rd, completely rev. edn., 1990.

[65] P. E. Ciddor, *Appl. Opt.*, 1996, **35**, 1566-1573.

[66] Reference Air Mass 1.5 Spectra (ASTM G-173-03), https://www.nrel.gov/grid/solar-resource/spectra-am1.5.html, (accessed Sep 26, 2022).

[67] D. Polak, R. Jayaprakash, T. P. Lyons, L. Á. Martínez-Martínez, A. Leventis, K. J. Fallon, H. Coulthard, D. G. Bossanyi, K. Georgiou, A. J. Petty II, J. Anthony, H. Bronstein, J. Yuen-Zhou, A. I. Tartakovskii, J. Clark and A. J. Musser, *Chem. Sci.*, 2020, **11**, 343-354.

[68] M. Wu, T.-A. Lin, J. O. Tiepelt, V. Bulović and M. A. Baldo, *Nano Lett.*, 2021, **21**, 1011-1016.

[69] Q. Liu, H. Liu, D. Li, W. Qiao, G. Chen and H. Ågren, *Nanoscale*, 2019, **11**, 14070-14078.

[70] L. Liang, D. B. L. Teh, N.-D. Dinh, W. Chen, Q. Chen, Y. Wu, S. Chowdhury, A. Yamanaka, T. C. Sum, C.-H. Chen, N. V. Thakor, A. H. All and X. Liu, *Nat. Commun.*, 2019, **10**, 1391.

Chapter 4 Conclusions and Future Remarks

4-1 Conclusions

This thesis focuses on developing efficient visible-to-UV photon upconversion systems using excited triplet states based on molecular diffusion.

Chapter 1 described a general introduction to photon upconversion and the basic information about TTA-UC. Furthermore, the current situation of visible-to-UV TTA-UC in solution, film, and solid systems was summarized.

In Chapter 2, an efficient UV-emitting acceptor, TIPS-Nph, was investigated and used to develop a solution system paired with $Ir(C6)_2(acac)$. The combination of TIPS-Nph as an acceptor and $Ir(C6)_2(acac)$ as a donor showed a high TTA-UC efficiency of 20.5% and a low threshold excitation intensity of 1.1 mW cm^{-2}. These properties were achieved by the fact that TIPS-Nph has a low triplet level and exhibits high fluorescence quantum yield and high singlet generation efficiency. In particular, the advantages of using $Ir(C6)_2(acac)$ allowed this system to demonstrate TTA-UC under a solar simulator and indoor LED, which indicates that this system has the potential for real-world applications of TTA-UC.

Chapter 3 introduced a simple porous film impregnation method to develop efficient film systems using a porous film and low-volatile upconverting solution for visible-to-UV TTA-UC. The film prepared by this method showed a high efficiency of 27.6% and a relatively low threshold excitation intensity of 20.4 mW cm^{-2}. These superior characteristics were mainly due to the reduction of the inner filter effect. Furthermore, by combining the film with a microlens array, which can focus the excitation light onto the film, a much lower threshold excitation intensity of less than 0.6 mW cm^{-2} was observed. The film prepared by this method can be applied to other TTA-UC chromophores and is expected to expand various applications.

4-2 Future remarks

Although TTA-UC materials that efficiently produce UV light have been developed in this thesis, upconversion performances can still be improved. For example, the acceptor singlet generation efficiency (f) could theoretically reach 40% or more, and some researchers have provided beneficial guidelines for the molecule design.[1, 2] These acceptors with high f values would enhance the efficiency of TTA-UC. In addition to improving intrinsic properties, developing whole solid systems showing a high efficiency under low excitation intensity is vital since TTA-UC systems containing organic solvents are not environmentally friendly and have low processability. That would be a barrier to the practical application of TTA-UC. The number of studies on solid-state systems is currently limited, and most are based on polymers as the matrix. While using polymers is a common strategy

for constructing solid-state materials, polymers likely to absorb UV light should be less compatible with visible-to-UV TTA-UC acceptors that exhibit UV emission. In addition, the low diffusion of the triplet states in polymer hampers efficient TET and TTA. These problems may be solved using a system in which the acceptor exhibits amorphous behavior in the solid state and behaves as a host material or using a porous acceptor crystal where donors can be introduced. Since the emission of the acceptor is different from its absorption location, the loss in the UV range can be reduced by adjusting the absorption characteristics. Furthermore, this higher density of acceptors should also result in better TTA-UC than solution or polymer systems because the triplet diffusion becomes energy diffusion rather than molecular diffusion.

4-3 References

[1] D. G. Bossanyi, Y. Sasaki, S. Wang, D. Chekulaev, N. Kimizuka, N. Yanai and J. Clark, *JACS Au*, 2021, **1**, 2188-2201.

[2] L. Naimovicius, E. Radiunas, M. Dapkevicius, P. Bharmoria, K. Moth-Poulsen and K. Kazlauskas, *J. Mater. Chem. C*, 2023, **11**, 14826-14832.